Self-management of the umbilical of a ROV for underwater exploration

Christophe Viel*

* CNRS, Lab-STICC, F-29806, Brest, France (e-mail: christophe.viel@ensta-bretagne.fr).

ARTICLE INFO

Keywords:
Underwater robotics, cables management, cables model

ABSTRACT

This article focuses on passive self-management of the umbilical of a Remotely Operated Vehicle (ROV) for underwater exploration. The goal is to give a predictable shape to the umbilical, using moving ballasts and buoys to stretch the umbilical and so to avoid entanglement of the cable itself or with surrounding obstacles. The ballasts and buoys move by themselves to maintain the cable taut without a motorized system. A model of the umbilical is proposed. The presence of waves, as well as the cases with and without currents are considered. Three configurations of the umbilical are proposed, each one to be the most adapted to ROV exploration missions: near the surface, sea exploration, and diving in presence of large obstacles.

1. Introduction

The underwater umbilicals are used to link an underwater Remotely Operated Vehicle (ROV) to a control unit or a Human-Machine Interface usually placed on a boat. This umbilical, or tether, can have three objectives: first the transmission of data in real time in both directions, *i.e*. real-time video feedback, control inputs, instrument measurements... (see [5, 19]), seconds provide energy to the ROV, third to avoid losing the robot during the exploration [17]. Umbilicals have however many drawback like collision with obstacles, umbilical inertia and drag forces impacting the maneuverability of the ROV, entanglement, cable breakage due to the vehicle's mass, etc... The umbilical's design is therefore a trade-off between the umbilical constraint, battery power and real-time feedback in the ROV performance [6].

The knowledge of the umbilical's shape has two main interests. First, designing the umbilical's parameters before the dive allows to avoid problems of weight, and to limit the risk of entanglement for example by avoiding the use of a cable unnecessarily too big or too long. Second, knowing the umbilical shape in real time during the dive allows an operator to prevent the self entanglement or with an obstacle already known in a mapped environment or detected by sensors (sonar, vision...). So in the literature, the umbilical has been modeled and instrumented to provide a feedback on its position and shape. Two main categories of methods exist in the literature: the detection of the umbilical using vision [15, 14, 16] and/or sensor placed directly on/in the umbilical to obtain a feedback on its shape [10, 7], or a direct modeling of the umbilical using only boat and ROV position [11, 12, 9], sometimes including an a-prior knowledge of the sea current. The main advantage of the first category is the accuracy of the estimated shape, often in real time. However, these strategies require specific umbilical equipments often expensive with a complex sensors' setup, making the modeling methods very attractive for a cheap obstacle avoidance. This second category of methods have also the advantage of being implementable for all kinds of umbilicals, but are often less accurate and cannot always provide results in real-time.

Several methods exist to model the cable's shape and dynamics, from simple geometrical models like catenary curve [20] to chains of segments with geometrical constraints like in [11]. These methods are perfect to simulate a large number of segments in real-time and are memory efficient when an accurate physical model is not necessary. When an accurate knowledge of the cable dynamic is required, the Lumped-mass-spring method [4, 12, 13] and the segmental method [8, 9, 2] are mostly used. The first method models the umbilical as mass points joined together by massless elastic elements, the second describes the cable as a continuous system and numerically solves the resulting partial differential equations.

The umbilical can also be equipped. A TMS (Tether Management System), a subsea winch controlled by a human operator and attached to the ROV cage [1], can so be used to regulate the amount of tether cable and thus keep the umbilical taut. This system is however heavy for the cable, and its operation can be a complex task. Some works try to automate or replace it by another vehicle like a USV [21], secondary ROV or several ROVs [16] or a motorized plug/float assembly [3]. However, all these systems require to be managed by an operator in real time, using the knowledge of several ROV's parameters, like the position.

This paper proposes a passive self-management of the umbilical of an ROV for underwater exploration using moving ballasts and buoys, without motorization. Since the shape of the umbilical can be complex to predict when it moves freely, we propose to add ballasts and buoys to introduce tension inside the cable and to stretch it, and so make its shape assimilated to predictable straight lines. In this perspective, this paper proposes:

- three equipments of the umbilical for three typical ROV missions: ship hull inspection and close-surface operation, exploration of seabed, and diving exploration in presence of large obstacles.

ORCID(s):

- to use ballasts and buoys to tend the umbilical and so to obtain a quasi-static equilibrium model of the umbilical, simple to compute in real time, and helping the operator to prevent collisions with environmental obstacles,
- the delimitation of areas where, thanks to the ballasts and buoys, the ROV can evolve without risk of cable's entanglement even in presence of currents,
- a method to choose the ballasts and buoys' parameters to counteract the waves' effects,
- a passive self-management of the umbilical without motorization or TMS.

In opposite with [3], the ballast and buoys are not motorized and move by themselves to maintain the cable taut using only weight and Archimedes' force. The umbilical is then modeled using geometrical relations and the fundamental principle of static, for an approach faster and lighter to compute than the lumped-mass-spring method or the segmental methods studied in [4, 12, 9, 8]. In absence of current, the only required knowledge is the ROV's position and a limitation of its acceleration in some directions. Cases with currents will require the knowledge of their force and their orientation to evaluate the shape of the umbilical, but this knowledge is are not required to evaluate areas where the absence of entanglement in the umbilical is guaranteed.

Section 2 exposes the related work. The problem's statement and the assumptions are described in Section 3. The management of the umbilical for surface exploration is presented in Section 4. The management of the umbilical for sea exploration without horizontal currents is exposed in Section 5. The subsections 5.2 describes the geometrical and static model. Restricted areas guaranteeing that the umbilical is always taut are also described in this section. The stiffness of the umbilical is studied in Section 5.5.1. The two-dimensional case with horizontal current is exposed in Section 6, followed by the three-dimensional case with horizontal current in Section 7. The last management case of the umbilical, for diving exploration in presence of large obstacles is shortly described in Section 8. The presence of waves is studied in Section 9, and Section 8 extends the obtained results to quasi-static equilibrium. Section 12 discuss of the validity of the chosen model and assumptions, based on pool experimentations. Finally, the Section 13 concludes this work.

2. Related work

2.1. Cable modeling

Several methods exist to model the cable's shape and dynamics. The simplest model is the catenary curve [20], referring to a non-rigid flexible cable whose weight the in water is greater than the buoyancy force. Nevertheless, when the cable is very long or heavy, more parameters like bending stiffness must be taken into account. In other methods like [11], neutrally buoyant cables are considered, allowing to ignore gravity and buoyancy forces. The umbilical is modeled as a long chain of segments, with geometrical constraints between them, to consider umbilical's stiffness. Although they are not necessarily physically accurate, and they do not consider the dynamics of the cable, these geometrical models allow a fast calculation and are memory efficient.

To obtain a dynamical and physically accurate cable model, two main kinds of methods exist [2]: the lumped-mass-spring method [4, 12, 13] and the segmental method [8, 9]. The first method models the umbilical as mass points joined together by massless elastic elements. This approach is very useful for elastic cables but requires large computational resources. The segmental method describes the cable as a continuous system and numerically solves the resulting partial differential equations. These two methods focus on the cable dynamics in simple environments with few forces: gravity, buoyancy, hydrodynamic drag, environment inertial force, axial tension, twisting force and bending force. In [9], a three-dimensional ROV-cable model is presented using Euler-Bernoulli's beam theory, modified to allow the compression of the cable. The model is verified experimentally.

2.2. Cable instrumentation

The umbilical can be equipped and instrumented to provide a feedback on its position and shape. Two main categories exist in the literature: the detection of the umbilical using vision [15, 14, 16], and the use of sensors placed directly on/in the umbilical [10, 7]. These methods allow an accurate model, often in real time, but requires specific umbilical equipment, often expensive and complex to install.

In [10], a method named "Smart Tether" gives the shape and the motion of the cable in real time using IMU sensor nodes embedded in the umbilical itself. The main inconvenient of this method, in addition to its price and the difficulty to set up the sensors, is that these nodes induce an irregular shape along the cable, causing problems for winding. In [7], optic fibers are braided within the umbilical and use the interferometry properties to monitor the curve of the whole cable in 3D in real time. Again, this solution has a very high cost again (about 200 000 euros for 50 m length).

For exploring shallow waters, [16] proposes an umbilical composed of mini-ROVs following each other. The shape of cable is controlled by i) the detection of the cable shape's using cameras behind the ROV through a color segmentation, see [15, 14], ii) the tracking of a constant distance between the successive ROVs. Umbilical 3-D shape parameters are estimated in real-time thanks to a curve fitting procedure based on the Gauss-Newton algorithm, then used inside the cable model based on a catenary model or a straight line.

Additional components such as TMS, ballasts, buoys or intermediate cables can also be used as dampers to avoid undesired forces on the ROV due to waves/currents or to the umbilical weight. For deep and ultra-deep-water operations for example, [18] proposes alternative configurations for minimizing the tension in the umbilical and reducing the

risk of snap, like installing a serie of floaters along the umbilical. Three different configurations are numerically investigated and compared. However, the floaters increase the offset of the ROV by making the cable more sensible to currents. The most classic equipment is the TMS, a kind of underwater winch attached to the ROV's cage which regulates the amount of tether [1]. It allows the robot to move in the working area while keeping the umbilical taut. When the TMS is placed underwater, it acts as a ballast to reduce the ROV offset due to current and wave. Finally, TMS cannot handle umbilicals equipped with buoys or ballasts.

Since the operation of a TMS is a complex task which can be similar to control a secondary ROV, some works try to automate it or to replace it by an other vehiche (USV, secondary ROV... see [16, 3, 21]). In [3], a motorized plug/float assembly moves on the umbilical to change the buoyancy of this one, even drops the ROV to become temporary an AUV. A winch on the boat regulates the cable length. If this system is efficient and allows an important adaptation, it is huge, expensive and can not be adapted for all kind of ROVs' applications. In [21], the system is composed of an USV with an embedded winch, an umbilical and an ROV, to offer several ways to manage the cable. The distance between the USV and the ROV is adapted to stretch or loose the umbilical and so to avoid collision between the umbilical and underwater obstacles. A method to model its mechanical behavior is proposed, based on a segmental method.

3. Problematic and hypothesis

Let us define the referential $\mathcal{R}$ of origin $O = (0, 0)$ corresponding to the coordinates of the boat where the first extremity of the umbilical is attached. $R = (x, y)$ are the coordinates of the ROV, corresponding to the second extremity of umbilical. The vertical axis is oriented downwards, so for two $\left(y_1, y_2\right)$, $y_1 > y_2$ means y_1 is deeper than y_2 and $y = 0$ corresponds to the sea surface.

In absence of tension between its two extremities, a cable takes an irregular shape only limited by its length and its stiffness. In most of the shallower dives, a ballast is hung on the umbilical at a defined length to stretch the cable between the boat and the ballast. When the ROV is too close to the ballast, the cable between them floats/falls freely, taking the shape of a bell, subject to entanglement. To pull the cable taut independently of the ROV position, we propose to add another item on the umbilical.

Since the buoys and ballasts move in opposite direction, alternating the attachment of buoys and ballasts on the cable is a good solution to stretch it. However, a ballast/buoy linked to several cables (two parts of the same umbilical in our case) at fixed distances can only taut one of them in most cases, or several, but only in particular configurations. In opposite, a ballast/buoy which can move freely along the cable will always stop its position at the lowest/highest point where it stretches the both parts of the cable simultaneously.

This paper proposes several configurations alternating ballasts and buoys, fixed or moving freely along the umbilical to stretch it. Its shape can so be assimilated to configurations of predictable straight lines, where the rigidity of the cable can be modeled by minimal angles between lines. The main advantage of this method is the umbilical is self-managed without motorization and without TMS, using only gravity and Archimedes' force, with a shape predictable at the equilibrium.

Some parameters and particular configurations must however be considered. A ballast heavier than a buoy can makes it dives, and opposite. The action of the ballast on the umbilical becomes equal to a pulley if it is in contact with the seabed, same remark with the buoy reaching the surface. Since a large number of configurations exist (different numbers of ballasts, buoys, distances fixed between them or sliding, difference of weight...) and most do not guarantee to stretch the umbilical satisfactorily, this paper focuses on three chosen configurations with good performances for three different missions: ship hull inspection and close-surface exploration, sea exploration, and diving exploration in presence of large obstacles. These configurations will be exposed in the next sections and are briefly illustrated in Figure 1.

The following assumptions are considered in all the study:

A1) The ratio mass/buoyancy of the umbilical is negligible compared to the ballasts' weight and the buoys' buoyancy used in the configuration.

A2) The length of the cable is such that it is reasonable to neglect the length variation of the umbilical, considered as constant.

A3) When the umbilical is taut, its geometry can be assimilated to straight lines between defined points, here the ballasts, the buoys, the boat and the ROV. The rigidity of the cable can be modeled by a minimal angle $\theta_{\min}$ between them, described in Section 5.5.1.

A4) The ROV is enough strong and controllable to compensate action of the ballasts and buoys and so the ROV's position (x, y) is perfectly fixed when ROV is not moving.

A5) Let $P = m_m g - \left(\rho_{water} V_m g + F_{cy,m}\right)$ be the force exerted by the ballast M used in our system, with m_m the mass of the ballast, g is the gravity constant, ρ_{water} the volumetric mass of the water, V_m the volume of the ballast, and $F_{cy,m}$ be the force exerted by the vertical current applied to the ballast M where $F_{cy,m} < 0$ pushes down to the seafloor and $F_{cy,m} > 0$ pushes up to the surface. One assumes that $P > 0$, *i.e.* the ballast's weight is strong enough to dive.

A6) Let $F_{bi} = \left(\rho_{water} V_{b_i} - m_{b_i}\right) g + F_{cy,b_i}$ be the force exerted by the buoy b_i used in our system, with m_{b_i} the mass of the buoy, V_{b_i} its volume, ρ_{water} the volumetric mass of the water, and F_{cy,b_i} the force of the vertical current applied to the buoy where $F_{cy,b_i} < 0$ pushes down to the seafloor and $F_{cy,b_i} > 0$ pushes up to the surface. One assumes that

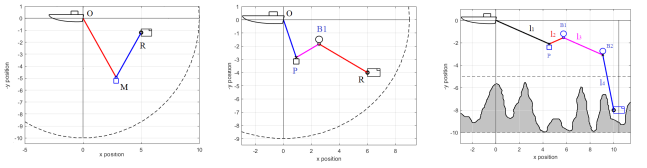

(a) Surface Exploration (b) Sea Exploration (c) Diving exploration

Figure 1: Methods exposed in this works. Square: ballast. Circle: buoy. "x": fixed ballast/buoy. "o": slidding ballast/buoy. Other parameters will be exposed in futur sections.

$\forall i \in [1 \dots N]$, $F_{b_i} > 0$, *i.e.* the buoy's buoyancy is stronger than its weight and the vertical current force.

A7) When a ballast/buoy is considered to move freely on the umbilical, one assumes that there is no friction between the umbilical and the ballast/buoy.

The validity of these assumptions in practical cases, specifically Assumption A4 and A7, will be discussed in Section 12. Remark: if hypothesis A5 or A6 are not respected, the ballast/buoy cannot act on the umbilical.

4. Umbilical for surface exploration

This section exposes a simple strategy of self-management of the umbilical to explore close to the surface, such as ship hull inspection, navigation under uniform ice floe, etc... In this configuration, the umbilical remains taut and below the ROV to not disturb it. This configuration is not adapted for seafloor exploration: next sections will proposed strategies for these cases.

Consider in this configuration an umbilical of length L with a sliding ballast M which can move freely between the two extremity of the umbilical, *i.e.* the ROV and the boat. Let α and β be respectively the oriented angle between the sliding ballast and the boat, and between the sliding ballast and the ROV. The parameters are illustrated on the Figure 2. In a configuration where the ballast is not in contact with the seabed or an obstacle, the umbilical is taut and the system can be expressed such

$$x = l_1 \sin(\alpha) - l_2 \sin(\beta) \tag{1}$$
$$y = l_1 \cos(\alpha) - l_2 \cos(\beta) \tag{2}$$

with $L = l_1 + l_2$ where $l_1 = ||OM||$ and $l_2 = ||MR||$.

If the environment is free of obstacles, the ROV can move in the area corresponding to the half circle $\mathcal{C}(O, L)$ of radius L and center O, so $x \in [-L, L]$ and $y \in [0, L]$. The ROV must however pass through the position $(0, L)$ to switch from the areas $[-L, 0]$ and $[0, L]$ without creating an entanglement around the ballast M which would block its displacement.

4.1. Configuration without horizontal current

Consider in a first time there is no horizontal current, vertical current being considered by Assumption A5.

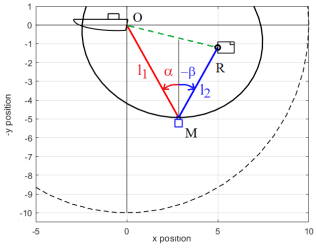

Figure 2: Parameters for Surface Exploration. M: sliding ballast. Black dash line: area where the ROV can move with its umbilical of length L. Black line: ellipse of centers O and R. Green dash line: longest diameter of the ellipse.

The ballast M is sliding freely on the umbilical of fixed length L, link to the boat and the ROV: due to the umbilical limitation, the ballast can be only inside the ellipse $\mathcal{E}_1$ of centers O and R and radius $r_1 = \frac{L}{2}$ and $r_2 = \sqrt{\left(\frac{L}{2}\right)^2 - \frac{x^2+y^2}{4}}$, and the umbilical is stretched only when the ballast is on the ellipse periphery, as illustrated in Figure 2. Considering Assumption A5 and A7, in absence of horizontal current and since the ballast is sinking, the ballast position is the lowest position and ellipse properties show that

$$\alpha = -\beta \tag{3}$$

Using (3), (1)-(2) becomes

$$x = L \sin(\alpha) \tag{4}$$
$$y = \left(l_1 - l_2\right) \cos(\alpha). \tag{5}$$

Since $x \in [-L, L]$ and $y \in [0, L]$, one can deduce from (4)-(5) that

$$\alpha = \operatorname{asin}\left(\frac{x}{L}\right) \tag{6}$$
$$l_1 = \frac{1}{2}\left(L + \frac{y}{\sqrt{1 - \left(\frac{x}{L}\right)^2}}\right) \tag{7}$$
$$l_2 = L - l_1 \tag{8}$$

Proofs of (6)-(8) are provided in [22, Appendix A.1].

Minimum seafloor depth or ROV diving

Let note y_{floor} the minimum depth inside the circle $\mathcal{C}(O, L)$ due to the environment, in most case the seafloor or a rock put on the sea floor. The system (4)-(5) is valid only if the ballast stretches the umbilical, so if the ballast has no contact with the seabed or with an obstacle. This condition is always satisfied if $y_{\text{floor}} \geq L$. In other case, since the ballast is always lower than the ROV level, let define the limit depth $y_{\text{lim}}(x)$ for a given position x which guarantee the ballast is always higher than y_{floor} if $y \leq y_{\text{lim}}(x)$.

In absence of current, following steps exposed in [22, Appendix A.2], $y_{\text{lim}}(x)$ can be expressed such

$$y_{\text{lim}}(x) = 2\left(y_{\text{floor}} - h_M\right) - L\sqrt{1 - \left(\frac{x}{L}\right)^2} \tag{9}$$

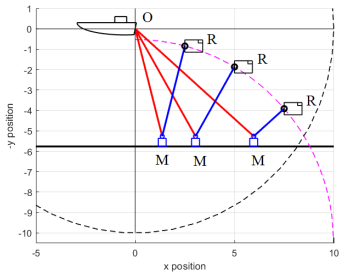

Figure 3: Limit depth y_{lim} which guarantee the ballast is not in contact with the seafloor for Surface Exploration. M: sliding ballast. The dash magenta line: y_{lim}. Large black line: seafloor y_{floor}. Red line: l_1. Blue line: l_2.

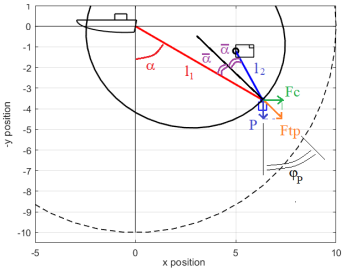

Figure 4: Parameters for Surface Exploration with horizontal current. M: sliding ballast. Black dash line: area where the ROV can move due to the umbilical length. Solid black line: ellipse of centers O and R and radius $\frac{L}{2}$ and $\sqrt{\left(\frac{L}{2}\right)^2 - \frac{x^2+y^2}{4}}$.

where h_M is the ballast height. (9) is illustrated in Figure 3. Remark also if the position x is unknown, a simple condition to guarantee its hypothesis is to take $y_{\text{lim}} = 2\left(y_{\text{floor}} - h_M\right) - L$.

4.2. Configuration with horizontal current

Consider now the presence of horizontal current. Let $F_{cx,m}$ be the force exerted by the horizontal current applied on the ballast M of mass m on the axis Ox, where $F_{cx,m} > 0$ corresponds to a current in the direction $\vec{Ox}$. Consider P the force exerted by the ballast respecting Assumption A5. Finally, let F_{tp} be the sum of force P and $F_{cx,m}$ with $\psi_{P,x}$ its orientation such

$$F_{tp} = \sqrt{P^2 + F_{cx,m}^2} \tag{10}$$

$$\psi_{P,x} = \text{atan}\left(\frac{F_{cx,m}}{P}\right). \tag{11}$$

Since the ballast M is still sliding on the umbilical, its position is on the ellipse $\mathcal{E}_1$ defined in Section 4.1 and so F_{tp} creates in the umbilical two angles $\bar{\alpha}$ identical as illustrated in Figure 4 such

$$\bar{\alpha} = \alpha - \psi_{P,x} \tag{12}$$

$$\bar{\alpha} = \psi_{P,x} - \beta \tag{13}$$

leading to

$$\alpha = 2\psi_{P,x} - \beta. \tag{14}$$

Remark (14) is equal to (3) when $F_{cx,m} = 0$. Using (14) and a rotation of the referential $\mathcal{R}$ as described in [22, Appendix A.3], one gets the new expression of the parameters:

$$\alpha = \text{asin}\left(\frac{x\cos\left(\psi_{P,x}\right) - y\sin\left(\psi_{P,x}\right)}{L}\right) + \psi_{P,x} \tag{15}$$

$$l_1 = \frac{1}{2}\left(L + \frac{y\cos\left(\psi_{P,x}\right) + x\sin\left(\psi_{P,x}\right)}{\sqrt{1 - \left(\frac{x\cos(\psi_{P,x}) - y\sin(\psi_{P,x})}{L}\right)^2}}\right) \tag{16}$$

and $l_2 = L - l_1$, $\beta = 2\psi_{P,x} - \alpha$.

A new limit depth y_{lim} noted $\bar{y}_{\text{lim}}$ can be defined in this configuration. However, since the current pushes the sliding ballast upward, the new limit depth $\bar{y}_{\text{lim}}$ is higher than y_{lim} described for case without current, *i.e.* $\bar{y}_{\text{lim}} \leq y_{\text{lim}}$. Since the current can be irregular making the position of M varying between its positions with and without current, it is recommend to use only y_{lim} as limit depth.

The same comment can be made for the 3 dimensions case. The presence of a current $F_{cz,m}$ perpendicular to the plan (O, x, y) pushes the sliding ballast upwards: the limit y_{lim} is so still a sufficient requirement to guarantee the sliding ballast will not touch the seafloor and so the umbilical will stay taut. Note the 3D model is not trivial to solve even for this simple configuration, but this sufficient requirement avoids to solve it. Note also 2D model is applicable for 3D case in absence of horizontal current by choosing the referential such $\vec{Ox}$ corresponding to the projection of $\vec{OR}$ on the surface, the ballast M being always inside (O, x, y) at the equilibrium.

5. Umbilical for Sea exploration without horizontal current

This section exposes a simple strategy of self-management of the umbilical to explore the sea and the seafloor. In this configuration, a ballast is fixed on the umbilical at a constant distance of the boat, and a buoy can move freely between the ballast and the ROV. The umbilical remains taut as long as the ROV does not enter in a defined forbidden area. In opposite with the strategy proposed in Section 4, the ROV can evolve close to the seafloor in a large area, but its movements are restricted when it is close to the surface. In this section, the problem is studied only for the two dimensional case (2D case) and without horizontal current. The presence of current will be added in Section 6 and three dimensional case (3D case) will be studied in Section 7.

5.1. Introduction of the geometrical model and restricted areas

Consider in this configuration an umbilical of length l divides in two parts: a first part of length l_1 between O and the

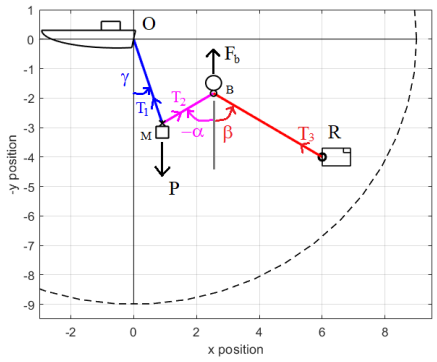

Figure 5: Parameters for Sea Exploration. M is the fixed ballast and B the sliding buoys. In the example here, $P = 3F_b$. The blue, magenta, red lines correspond to l_1, l_2, l_3. Black dash line: area where the ROV can move with its umbilical length.

ballast M fixed on the umbilical, *i.e.* $\|OM\| = l_1$, and a second part of length L where the buoy B can move freely between the ballast and the ROV. Similarly to the problem studied in Section 4, L can be divided in two lengths $l_2 = \|MB\|$ and $l_3 = \|BR\|$ corresponding to the lengths of the left side and right side of the buoy, where $L = l_2 + l_3$. Let γ be the oriented angle between the boat and the ballast M. The oriented angles α and β are respectively the angle between the ballast and the buoy, and between the buoy and the ROV. Parameters are illustrated in Figure 5.

Since the ROV can not go higher than the sea level and to avoid node between l_1 and L, the ROV can move in the area corresponding to the quarter of the circle $\mathcal{C}(O, l)$ of radius $l = l_1 + L$ and center O, so $x \in [0, l]$ and $y \in [0, l]$ (the area $x \in [-l, 0]$ will be discussed later in the section). In a configuration where the umbilical is taut, the system can be expressed such

$$x = l_1 \sin(\gamma) - l_2 \sin(\alpha) + l_3 \sin(\beta) \tag{17}$$
$$y = l_1 \cos(\gamma) - l_2 \cos(\alpha) + l_3 \cos(\beta) \tag{18}$$
$$L = l_2 + l_3. \tag{19}$$

where l_1 and L are fixed and known, $L \geq l_2 \geq 0$ and $L \geq l_3 \geq 0$.

Similarly to the problem studied in Section 4, the buoy finds its position on the ellipse $\mathcal{E}_2$ as long as it does not touch the surface (this condition will be studied below). M and R are the centers of $\mathcal{E}_2$, with the two radius $\frac{L}{2}$ and $\sqrt{\left(\frac{L}{2}\right)^2 - \frac{(x-x_M)^2+(y-y_M)^2}{4}}$ where (x_M, y_M) are the coordinates of the ballast M. In absence of horizontal current, ellipse properties show that

$$\alpha = -\beta. \tag{20}$$

In function of the ROV position, six areas corresponding to specific umbilical configurations can be observed, illustrated in Figure 6:

- Area A: standard behavior of the system. The umbilical is perfectly taut by the action of the ballast and the buoy with $\gamma > 0$, $l_2 > 0$, $l_3 > 0$.
- Area B: the buoy is on the surface but the ballast can still taut the cables l_1 and L, with $\gamma \geq 0$, $l_2 > 0$, $l_3 > 0$. Note Area B does not exist if $L < l_1$.
- Area C: two cases are possibles
  - if $L \geq l_1$, the buoy is on the surface and ballast can not taut the cable L,
  - if $L < l_1$, the cable l_1 is not taut because the ROV is too close to the surface for the ballast can stretch l_1 and L (the only solution of the system (17)-(19) is $\gamma < 0$ for $x > 0$, impossible in practice without horizontal current). Moreover, the buoy is in contact with the ROV.
- Area D1: the umbilical is taut and the buoys is in contact with the ROV, so $l_2 = L$ and $l_3 = 0$.
- Area D2: the umbilical is taut and the buoys is in contact with the ballast M: $l_2 = 0$ and $l_3 = L$.
- Area E: area inaccessible due to the length l.

The system is considered to be inside an area if the ROV coordinate (x, y) is inside this area. The ROV must not enter in area C because the umbilical cannot be taut inside, making the model (17)-(19) invalid and allowing the appearance of entanglements. In case where this strategy of self-management of the umbilical is used without need to model the umbilical in real time, the operator only need to know areas C and E. All areas are required only to model the umbilical, its shape being different in each area.

Following steps described in in [22, Appendix B.6], the boundaries between area A and the others areas can be expressed as

$$y_{area\,B}(x) = \begin{cases} \max\left(\frac{L - l_1\sqrt{1+(\Lambda^2-1)\sin(\gamma_A(x))^2}}{\sqrt{1+\Lambda^2\tan(\gamma_A(x))^2}}, 0\right) + h_B & \text{if } L \geq l_1, \\ h_B & \text{else.} \end{cases} \tag{21}$$

$$y_{area\,C}(x) = \begin{cases} \sqrt{l_1^2 - x^2} - L + h_B & \text{if } \left(|x| < \sqrt{l_1^2 - L^2}\right) \,\&\, \left(l_1 > L\right), \\ \sqrt{L^2 - x^2} - l_1 + h_B & \text{if } \left(|x| < \sqrt{L^2 - l_1^2}\right) \,\&\, \left(L > l_1\right), \\ h_B & \text{else.} \end{cases} \tag{22}$$

$$y_{area\,D1}(x) = \max\left(\frac{l_1\sqrt{1 + \left(\Lambda^2 - 1\right)\sin\left(\gamma_A(x)\right)^2} - L}{\sqrt{1 + \Lambda^2\tan\left(\gamma_A(x)\right)^2}}, 0\right) \tag{23}$$

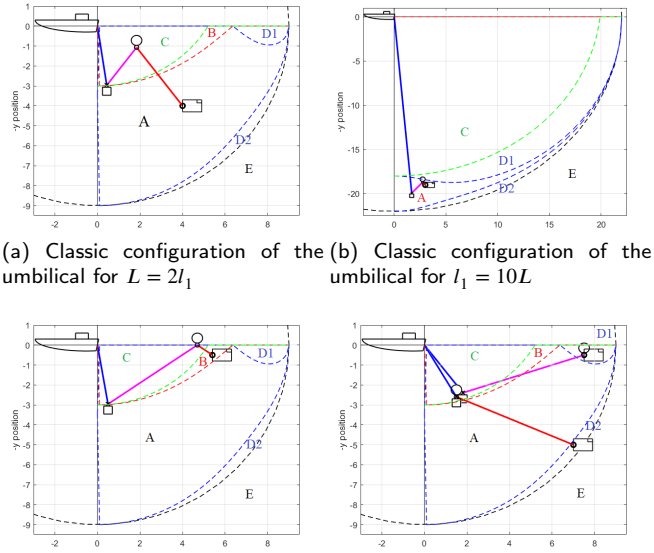

(a) Classic configuration of the umbilical for $L = 2l_1$

(b) Classic configuration of the umbilical for $l_1 = 10L$

(c) Buoy on the surface with l_1 still stretch ($\gamma > 0$).

(d) Buoy in contact with the ballast ($l_2 = 0$, $l_3 = L$) or the ROV ($l_2 = L$, $l_3 = 0$)

Figure 6: Different areas for Sea Exploration. Green dash line: area C. Red dash line: area B. Blue dash lines : areas D1 and D2. Black dash line: area E. Note area B does not exist in sub-figure b.

$$y_{area\ D2}(x) = \max\left(\frac{l_1\sqrt{1+\left(\Lambda^2-1\right)\sin\left(\gamma_A(x)\right)^2}+L}{\sqrt{1+\Lambda^2\tan\left(\gamma_A(x)\right)^2}}, 0\right) \tag{24}$$

$$y_{area\ E}(x) = \sqrt{l^2-x^2}. \tag{25}$$

where γ_A is the evaluation of γ inside area A, as it will be described in Section 5.3, and h_B is the height of the submerged part of the buoy when the buoy floats freely on the surface without constraints.

Area B converges to area C when the ration $\frac{P}{F_b}$ increases, and area C increases with the discrepancy between l_1 and L, to not exist if $l_1 = L$. Note areas C and E depend only of l_1, L and x, so can be modeled easily.

Minimum seafloor depth

The previous areas show the minimum depth where the ROV must dive to guarantee the umbilical stay taut due to the presence of the buoy, but assumes that the depth is sufficient in all cases. In practice, conditions on the minimum deep y_{floor} must also be respected.

Let note y_{floor} the minimum depth inside the circle $C(O, l)$. The system (17)-(18) is valid only if the two following conditions are respected

1. The ballast has no contact with the seabed or with an obstacle during its displacement, so y_{floor} must be lower than the circle of center O and radius l_1,
2. The ROV does not go inside area C defined previously, so $y_{\text{floor}}(x) \geq y_{area\ C}(x)$.

Thus, for a given position x, the minimum seafloor depth $y_{\text{floor}}(x)$ can be expressed as

$$y_{\text{floor}}(x) \geq \max\left(\left[y_{area\ C}(x), y_{\text{ballast}}(x)\right]\right) \tag{26}$$

where

$$y_{\text{ballast}}(x) = h_M + \sqrt{l_1^2 - x^2} \tag{27}$$

with h_M is the ballast height. Note (26) is always satisfied if the seafloor respects the following condition

$$y_{\text{floor}} \geq h_M + \max\left(\left[l_1, L - l_1\right]\right). \tag{28}$$

5.2. Static model

In this section, the ROV is supposed to be inside area A. Results exposed are not valid in others areas, which will be studied in next sections.

In system (17)-(20), the unknown parameters are l_2, l_3, α, β and γ. Since the system (17)-(20) provides 4 equations, a last one must be found. Let define P and F_b the force applied on the umbilical by the ballast and the buoy, following assumptions A5 and A6. Moreover, suppose the ballast and the buoy are chosen respecting the following Assumption A8:

Assumption A8) The masses and buoyancy of the ballast and the buoy are chosen such

$$P \geq F_b \max\left(\left[1, \frac{1}{2}\left(\frac{l_1}{L}+1\right)\right]\right). \tag{29}$$

This constraint will be shown and used in the appendices, and are only used in this section and Section 6 (case with horizontal current).

Considering Assumptions A1 to A8, let perform the Fundamental Principle of Static (FPS) on M and B, as illustrates in Figure 5:

$$\Sigma_M \vec{F} = P\vec{y} + \vec{T}_1 + \vec{T}_2 \tag{30}$$

$$\Sigma_B \vec{F} = -F_b\vec{y} - \vec{T}_3 - \vec{T}_2 \tag{31}$$

where $\vec{T}_1$, $\vec{T}_2$ and $\vec{T}_3$ are the tension of the umbilical applied on the ballast and the buoy.

Following steps described in [22, Appendix B.2], one can show that

$$\tan(\beta) = \Lambda\tan(\gamma). \tag{32}$$

where $\Lambda = 2\frac{P}{F_b} - 1$ and remark $\Lambda \geq 1$ because $P \geq F_b$.

Adding (32) to (17)-(20), One now has enough equations to solve the system inside area A.

5.3. Umbilical model solved in area A

In this section, let's consider the ROV is inside area A. The Theorem 1 describes the value of parameters γ, α, β, l_2 and l_3. For this section and the following ones, let not γ_A the evaluation of γ inside area A, as described in the following theorem.

Theorem 1. *Consider the system (17)-(19) with* $(x, y) \in [0, l]^2$ *and where* (x, y) *is inside area A, i.e.* $l_2 > 0$, $l_3 > 0$. *Considering also the Assumption A8 and the absence of horizontal current, i.e. (32) and (20). The angle* γ *can be expressed* $\gamma = \gamma_A$ *such*

a) if $x = 0$, *the only geometrical solution without current is* $\gamma_A = 0$,

b) if $P = F_b$, *one has* $\Lambda = 1$ *and* γ_A *can be expressed as*

$$\sin\left(\gamma_A\right) = \frac{x}{l}. \tag{33}$$

c) if $P > F_b$ *and* $x > 0$, γ_A *can be expressed as*

$$\sin\left(\gamma_A\right) = \min_{i\in[1,2,3,4]}\left(\left|X_i\right|\right) \tag{34}$$

where

$$\begin{cases} X_1 = \frac{\sqrt{U-\frac{2}{3}A}-\sqrt{\Delta_{Y1}}}{2},\ X_2 = \frac{\sqrt{U-\frac{2}{3}A}+\sqrt{\Delta_{Y1}}}{2} & \text{if } \Delta_{Y1} \geq 0, \\ X_1 = \infty,\ X_2 = \infty & \text{else,} \end{cases} \tag{35}$$

$$\begin{cases} X_3 = \frac{-\sqrt{U-\frac{2}{3}A}-\sqrt{\Delta_{Y2}}}{2},\ X_4 = \frac{-\sqrt{U-\frac{2}{3}A}+\sqrt{\Delta_{Y2}}}{2} & \text{if } \Delta_{Y2} \geq 0, \\ X_3 = \infty\ X_4 = \infty & \text{else,} \end{cases} \tag{36}$$

with $\Delta_{Y1} = -\left(U + \frac{4}{3}A + \frac{2B}{\sqrt{U-\frac{2}{3}A}}\right)$,

$\Delta_{Y2} = -\left(U + \frac{4}{3}A - \frac{2B}{\sqrt{U-\frac{2}{3}A}}\right)$ *and*

$$A = -\frac{x^2}{2l_1^2} - \frac{\left(L^2\Lambda^2 - l_1^2\right)}{l_1^2\left(\Lambda^2-1\right)} \tag{37}$$

$$B = -\frac{l_1^2 + L^2\Lambda^2}{l_1^3\left(\Lambda^2-1\right)}x \tag{38}$$

$$C = \frac{x^4}{16l_1^4} + \frac{x^2\left(l_1^2 - L^2\Lambda^2\right)}{4l_1^4\left(\Lambda^2-1\right)} \tag{39}$$

$$U = \begin{cases} \left(-\frac{q}{2} + \sqrt{\frac{q^2}{4}+\frac{p^3}{27}}\right)^{1/3} + \left(-\frac{q}{2} - \sqrt{\frac{q^2}{4}+\frac{p^3}{27}}\right)^{1/3} & \text{if } \Delta_U > 0, \\ 2\cos\left(\frac{1}{3}acos\left(-\frac{q}{2\sqrt{-\frac{p^3}{27}}}\right)\right)\sqrt{-\frac{p}{3}} & \text{if } \Delta_U < 0, \\ \sqrt{-\frac{p}{3}} & \text{if } \Delta_U = 0 \end{cases} \tag{40}$$

and $\Delta_U = \frac{q^2}{4} + \frac{p^3}{27}$, $p = -4C - \frac{A^2}{3}$ *and* $q = \frac{2A^3}{27} + \left(4AC - B^2\right) + \frac{-4CA}{3}$. *Moreover, other parameters can be expressed such*

$$\beta = atan\left(\Lambda\tan\left(\gamma_A\right)\right) \tag{41}$$

$$l_2 = \frac{L}{2} - \frac{y - l_1\cos\left(\gamma_A\right)}{2\cos\left(\beta\right)}, \tag{42}$$

and $l_3 = L - l_2$, $\alpha = -\beta$.

The proofs of Theorem 1 are described in [22, Appendix B.3 and B.4]. If several configurations must be considered to evaluate γ in Theorem 1, a solution always exists and the solution is analytic, so can be evaluated quickly.

The Theorem 1 is evaluated for $x \geq 0$. Since the system (17)-(19) is symmetric for $[0, x]$ and $[-x, 0]$ in absence of horizontal current, the following corollary can be made.

Corollary 1. *In absence of horizontal current, the system (17)-(19) is symmetric for* $[0, x]$ *and* $[-x, 0]$, *and the Theorem 1 can be extended to the case* $x < 0$ *by taking* $|x|$ *instead of* x *inside the Theorem 1 and take the solution* $\sin\left(\gamma_A\right) = \min_{i\in[1,2,3,4]}\left(\left|X_i\right|\right) sgn\left(x\right)$.

If Corollary gives a solution for areas $(x, y) \in [0, l] \times [0, l]$ and $(x, y) \in [-l, 0] \times [0, l]$, the ROV must however pass through the position $(0, L)$ to switch from the two areas to avoid entanglement around the buoy B, which would block its displacement.

5.4. Umbilical model solved for all areas

The different areas must be considered because they represent particular geometrical configurations. In areas D1 or D2 for example, angle β or α does not exist because the distances l_2 or l_3 are equal to zero. Let first define γ_D the value of γ outside area A:

1) If $y \neq 0$, γ_D can be expressed as

$$\sin\left(\gamma_D\right) = \frac{a_D b_D - \sqrt{a_D^2 b_D^2 - \left(1+b_D^2\right)\left(a_D^2-1\right)}}{\left(1+b_D^2\right)} \tag{43}$$

with $a_D = \frac{x^2+y^2+l_1^2-L^2}{2yl_1}$ and $b_D = \frac{x}{y}$.

2) else, $y = 0$, γ_D can be expressed as

$$\sin\left(\gamma_D\right) = \frac{x^2 + l_1^2 - L^2}{2l_1 x}. \tag{44}$$

Note one has $x \neq 0$ because the ROV can only be inside area A or C if $x = 0$, so γ_D does not exist if $x = 0$.

The following Theorem 2 exposes the evaluation of the parameters γ, α, β, l_2 and l_3 in function of the area where the ROV is located.

Theorem 2. *Consider the system (17)-(19) for* $(x, y) \in [0, l]^2$ *and* $y < y_{area\,E}(x)$. *Considering the assumption A8 and the absence of current, i.e. (32) and (20), one gets*

(1) if $y < y_{area\,C}(x)$, *the model is not valid and the system (17)-(19) cannot be solved.*

(2) else if $y_{area\,B}(x) \neq 0$ *and* $y_{area\,C}(x) \leq y \leq y_{area\,B}(x)$, *then* (x, y) *is inside area B and one has* $\gamma = \gamma_D(x)$, $l_2 = L - l_3$ *and*

$$\cos\left(\beta\right) = \frac{y + l_1\cos\left(\gamma_D\right)}{L} \tag{45}$$

$$l_3 = \frac{Ly}{l_1\cos\left(\gamma_D\right) + y}. \tag{46}$$

(3) else if $y_{area\,D1}(x) \neq 0$ *and* $y_{area\,C}(x) \leq y \leq y_{area\,D1}(x)$, *then* (x, y) *is inside area D1 and one has* $l_2 = L$, $l_3 = 0$, $\beta = 0$, $\gamma = \gamma_D(x)$ *and*

$$\alpha = -acos\left(\frac{-y + l_1 \cos(\gamma_D)}{L}\right). \tag{47}$$

(4) else if $y_{area\,D2}(x) \leq y$, *then* (x, y) *is inside area D2 and one has* $l_2 = 0$, $l_3 = L$, $\alpha = 0$, $\gamma = \gamma_D(x)$ *and*

$$\cos(\beta) = \frac{y - l_1 \cos(\gamma_D)}{L}. \tag{48}$$

(5) else, then (x, y) *is inside area A and one has the parameters defined in Theorem 1 such* $\gamma = \gamma_A(x)$, $\alpha = -\beta$, $l_3 = L - l_2$ *with* $\tan(\beta) = \Lambda \tan(\gamma_A)$ *and* $l_2 = \frac{L}{2} - \frac{y - l_1\cos(\gamma_A)}{2\cos(\beta)}$.

The proofs of previous results are described in [22, Appendix B.7]. Note if Theorem 2 (1) is true, the ROV must dive to $y = y_{area\,C}(x)$ to make the system valid. Remark also case $y > y_{area\,E}(x)$ is not physically possible due to the umbilical length.

The Theorem 2 is evaluated for $x \geq 0$. Again, since the system (17)-(19) is symmetric for $[0, x]$ and $[-x, 0]$ in absence of horizontal current, the following corollary can be made.

Corollary 2. *In absence of horizontal current, the system (17)-(19) is symmetric for* $[0, x]$ *and* $[-x, 0]$, *and the Theorem 2 can be extended to the case* $x < 0$ *by doing the following changes :*

1) take $|x|$ *instead of* x *in Theorem 1 and (43) for the evaluation of* γ_A *and* γ_D,

2) take the solution $\sin(\gamma_A) = \min_{i\in[1,2,3,4]}(|X_i|)\, sgn(x)$ *in Theorem 1 and* $\sin(\gamma_D) = \frac{a_D b_D - \sqrt{a_D^2 b_D^2 - (1+b_D^2)(a_D^2-1)}}{(1+b_D^2)} sgn(x)$ *in (43),*

3) take the value $\beta = \beta sgn(x)$ *for cases (2)-(4) in Theorem 2.*

5.5. Practical case

5.5.1. model of umbilical rigidity and security angle

In practice, the umbilical has a rigidity which does not allow angles $|\alpha| + |\gamma|$ and $|\alpha| + |\beta|$ to become smaller than a minimum value. This rigidity can lead to collisions between the different part of the umbilical, as illustrated in Figure 8. To guarantee the absence of collision with the cable itself, this rigidity can be taken into consideration by introducing conditions $|\alpha| + |\beta| \geq \theta_{\min}$ and $|\alpha| + |\gamma| \geq \theta_{\min}$, or a minimum distance $x_{\min}$ to respect such $x > x_{\min}$.

Let define R_{curve} the cable rigidity, such $D = 2\pi R_{curve}$ is the perimeter of the smallest circle which can be performed with the umbilical, see Figure 7. To guarantee the absence of collision in the umbilical, the distance x must allow the cable to perform two half circles around the ballast and the buoy, and a quarter of circle at the connection between the ROV and the umbilical, as illustrated in Figure 8. It is considered the umbilical drops straight without problem of rigidity problem at the boat level. Thus, the distance x must be larger than

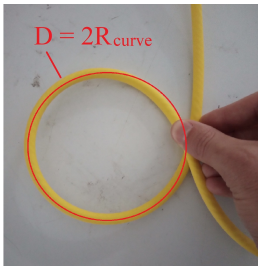

Figure 7: Characterization of umbilical rigidity

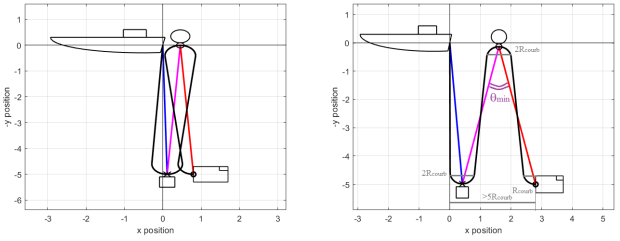

(a) Collision due to umbilical rigidity (b) Absence of collision

Figure 8: Umbilical shape considering its rigidity. Black line: shape of the umbilical due to cable rigidity. Blue: l_1. Magenta: l_2. Red: l_3. In the example here, $R_{curve} = 0.4$m and $l = 15$m.

$$x_{\min} = 5R_{curve}. \tag{49}$$

From (32) and Theorem 2, one has $|\gamma| \leq |\beta|$ in all cases. The minimum angle $\theta_{\min} = |\alpha| + |\beta| = 2|\beta|$ guaranteeing the absence of collision can so be defined such that

$$\theta_{\min} = 2\text{asin}\left(\frac{4R_{curve}}{L}\right). \tag{50}$$

(50) is shown in [22, Appendix B.1] and $\theta_{\min}$ is respected if $x \geq x_{\min}$. Note the value of $\theta_{\min}$ can be oversize for safety or for taking into account some other constraint, for example the presence of an optical fiber inside the umbilical requiring a larger curve to not break.

The parameter $\theta_{\min}$ will be more used in future sections in presence of horizontal currents.

5.5.2. Forces applied on the ROV

This section exposes the forces applied by the umbilical on the ROV, to choose the ballast and the buoy in the capabilities of the ROV. Let $\vec{F}_{cable\to ROV}$ be the force applied by the umbilical on the ROV and $\vec{T}_3 = -\vec{F}_{cable\to ROV}$ where $\vec{T}_3$ is exposed in Section 5.2. Then, one has from (31)

$$\Sigma_B \vec{F}.\vec{x} = 0 \tag{51}$$

$$-T_2 \sin(-\alpha) + T_3 \sin(\beta) = 0 \tag{52}$$

$$T_3 \sin(\beta) = -T_2 \sin(\alpha). \tag{53}$$

Since $\alpha = -\beta$, one has $T_3 = T_2$. Moreover, since $F_{cable\to ROV} = T_3$ and $T_2 = F_b \frac{\sin(\beta)}{\sin(2\beta)} = \frac{F_b}{2}\tan(\beta)$ from [22, Appendix B.2], one gets

$$F_{cable\to ROV} = \frac{F_b}{2\cos((\beta)}. \tag{54}$$

Deduce from (54) and Theorem 2 that $F_{cable\to ROV}$ increases with the distance $d = \sqrt{x^2+y^2}$. Since β is independent of y in area A (see Theorem 2), one deduces that $F_{cable\to ROV}$ increases only with x in area A.

5.5.3. Choice of umbilical length

Previous sections describe the umbilical shape and areas in function of predefined parameters like the umbilical length l. In practice, an operator searches the best umbilical length to explore an area approximately known. This section proposes a simple method to choose the parameters l, L and l_1 in function of several environmental constraints. More elaborate algorithms are proposed in [22, Appendix H], and others choices can be made.

Let's define $\left[y_{\min}, y_{\max}\right]$ the desired minimum depth and maximum depths for the ROV exploration, where $y_{\max} \leq y_{\text{floor}} - h_M$. Let's also define $\left[x_{\min}, x_{\max}\right]$ the desired minimum and maximum horizontal distances for the ROV exploration, where $x_{\min}$ has been defined in Section 5.5.1. Compromises must be made because not all the parameters $x_{\max}$, $y_{\min}$, $y_{\max}$ will be respected simultaneously. In this perspective, since the boat can move on the surface, the respect of parameters $\left[y_{\min}, y_{\max}\right]$ is favored over $\left[x_{\min}, x_{\max}\right]$.

To go the deepest possible without the ballast touching the seafloor, take $l_1 = y_{\text{floor}} - h_B$. Then,

- if $y_{\min}$ is favored over $y_{\max}$, take $L = l_1 + y_{\min}$, and $l = L + l_1$. To respect $y_{\min}$ for all $x \leq x_{\max}$, one takes $x_{\max} = \sqrt{l^2 - y_{\min}^2}$ and has $y_{\max}(x) = \sqrt{l^2 - x^2}$.
- if $y_{\max}$ is favored over $y_{\min}$ and respected for all $x \leq x_{\max}$, takes $L \in \left[\sqrt{y_{\max}^2 + x_{\max}^2} - l_1, 2l_1\right]$ with $x_{\max} = \sqrt{9l_1^2 - y_{\max}^2}$. One has $y_{\min}(x) = y_{area\,C}(x)$.

The umbilical respected simultaneously $y_{\min}$ and $y_{\max}$ for $x \in \left[x_{\min}, x_{\max}\right]$ if there exist L such

$$\sqrt{y_{\max}^2 + x_{\max}^2} - l_1 \leq L \leq l_1 + y_{\min}, \tag{55}$$

which is possible iff

$$x_{\max} \leq \sqrt{\left(2l_1 + y_{\min}\right)^2 - y_{\max}^2} \tag{56}$$

where $x_{\max} \geq 0$ because here $l_1 = y_{\text{floor}} - h_B \geq y_{\max}$.

6. Umbilical for Sea exploration with current

This section extends results of the configuration studied in Section 5 by adding presence of horizontal current. The presence of currents makes the system asymmetric and changes the position of the ballast and buoy, as well as the shape of areas exposed in the previous section.

6.1. Influence of current on the geometrical model

Consider the same configuration exposed in Section 5, and remind the presence of a vertical current is considering inside P and F_b, see Assumption A5 and A6. Let $F_{cx,m}$ and $F_{cx,b}$ be the forces of the current horizontal applied on the ballast M and buoy B on the axis $\vec{O}x$ such $F_{cx,m} > 0$ corresponds to a current in the direction $\vec{O}x$, same for $F_{cx,b}$, as illustrated on Figure 9. Let also define $F_{tm,x}$ and $F_{tb,x}$ such

$$F_{tm,x} = \sqrt{P^2 + F_{cx,m}^2} \tag{57}$$

$$F_{tb,x} = \sqrt{F_b^2 + F_{cx,b}^2} \tag{58}$$

with their incidence angles

$$\tan\left(\psi_{P,x}\right) = \frac{F_{cx,m}}{P} \tag{59}$$

$$\tan\left(\psi_{B,x}\right) = -\frac{F_{cx,b}}{F_b}. \tag{60}$$

Since the buoy is still moving freely on the umbilical and does not touch the surface (not inside areas B and C), its position is still on the ellipse $\mathcal{E}_2$ described in Section 5. In presence of horizontal current, ellipse properties shows that two angles $\bar{\alpha}$ identical are created by the force $F_{tb,x}$ such $\bar{\alpha} = \alpha - \psi_{B,x}$ and $\bar{\alpha} = \psi_{B,x} - \beta$, illustrated on Figure 9. This property leads to

$$\alpha = 2\psi_{B,x} - \beta. \tag{61}$$

Remark (61) becomes equal to (3) when $F_{cx,b} = 0$.

6.2. Static model with horizontal current

In this section, the ROV is supposed to be inside area A. Results exposed here are not valid in others areas, which will be studied in next sections.

Let perform the FPS on M and B with the presence of horizontal current as illustrated in Figure 9 (a):

$$\Sigma_M \vec{F} = \vec{F}_{tm,x} + \vec{T}_1 + \vec{T}_2 \tag{62}$$

$$\Sigma_B \vec{F} = \vec{F}_{tb,x} - \vec{T}_3 - \vec{T}_2 \tag{63}$$

Following [22, Appendix C.1], one gets

$$F_{tm,x} \frac{\sin(\Gamma)}{\sin\left(\Gamma + B + \Delta\psi_x\right)} = F_{tb,x} \frac{\sin(B)}{\sin(2B)}. \tag{64}$$

and

$$\tan(B) = \frac{\left(2\frac{F_{tm,x}}{F_{tb,x}} - \cos\left(\Delta\psi_x\right)\right)\tan(\Gamma) - \sin\left(\Delta\psi_x\right)}{\cos\left(\Delta\psi_x\right) - \tan(\Gamma)\sin\left(\Delta\psi_x\right)}. \tag{65}$$

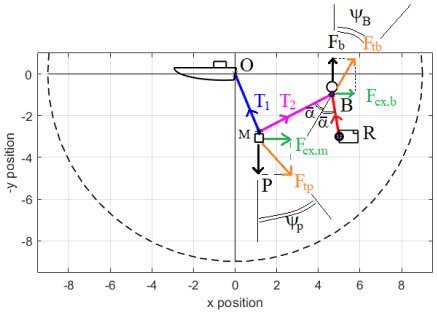

(a) $F_{cx,m} > 0$ and $F_{cx,b} > 0$

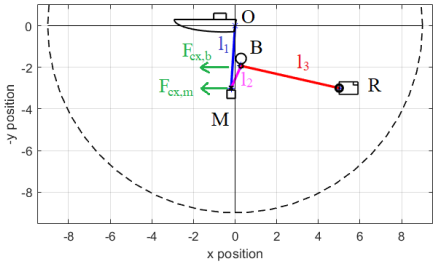

(b) $F_{cx,m} < 0$ and $F_{cx,b} < 0$

Figure 9: Parameters for Sea Exploration with current. M is the fixed ballast, B is the sliding buoys, such $P = 3.4F_b$ and $F_{cx,m} = F_{cx,b} = 0.5F_b$. The blue, magenta, red lines correspond to l_1, l_2, l_3. Black dash line: area where the ROV can move due to the umbilical length.

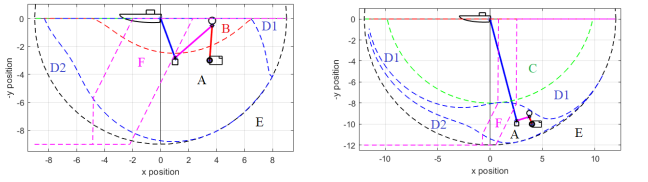

(a) Classic configuration, $L = 2l_1$ (b) Classic configuration, $l_1 = 10L$

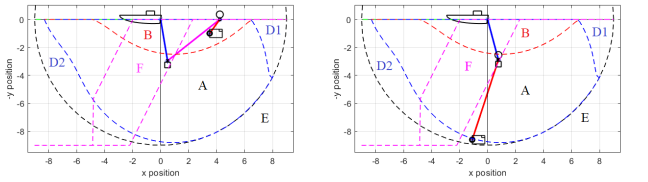

(c) Buoys on the surface with l_1 still taut. (d) Buoys in contact with ballast M: $l_2 = 0$ and $l_3 = L$.

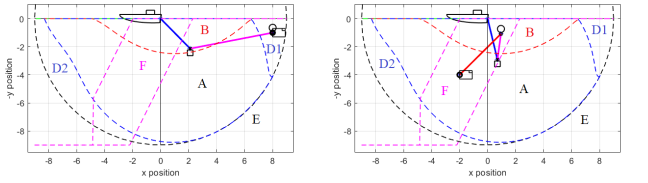

(e) Buoys in contact with ROV: $l_2 = L$ and $l_3 = 0$. (f) Cables l_1 and l_3 crossed. and action of the current.

Figure 10: The different areas for Sea Exploration with current. M: fixed ballast, B: sliding buoys. $P = 3F_b$, and $F_{cx,m} = F_{cx,b} = 0.5F_b$. Black dash line: area where the ROV can move due to the umbilical length. Note area B does not exist in sub-figure b where $L < l_1$ and area C does not exist in sub-figure where $L > l_1$.

with $\Gamma = \gamma - \psi_{P,x}$, $B = \beta - \psi_{B,x}$ and $\Delta\psi_x = \psi_{P,x} - \psi_{B,x}$. Note if $F_{cx,m} = 0$ and $F_{cx,b} = 0$, one has $\psi_{P,x} = 0$ and $\psi_{B,x} = 0$, so (65) is equal to (32).

6.3. Boundaries of areas

As illustrated in Figure 10, the six areas defined in previous Section 5 still exist. However, since the ballast and the buoy are pushed in the same direction than the current, the areas are not symmetric, and area C does not exist theoretically when $L > l_1$ because the umbilical can always be taut by the current. Following step from [22, Appendix C.2.1] and in presence of horizontal current, $y_{area\,C}(x)$ can be expressed as

$$y_{area\,C}(x) = \begin{cases} \sqrt{l_1^2 - x^2} - L + h_B & \text{if } \left(|x| < \sqrt{l_1^2 - L^2}\right) \,\&\, \left(l_1 > L\right), \\ h_B & \text{else} \end{cases} \tag{66}$$

It is however recommended to use area C described in Section 5 for the case without horizontal current in practice, specifically if the current is weak.

Due to the strong non-linearity of the relation (65), only a numerical approach has been found to find a boundary of areas B, D1 and D2, described in [22, Section 6.3]. However, the evaluation of boundaries of area B, D1 and D2 are not necessary to consider their influence in the model (17)-(19): using α_A, β_A and l_{3A} which will be evaluated with Theorem 3 in Section 6.4, one can deduce

- if $y \geq l_{3A}\cos\left(\beta_A\right)$, the ROV is inside area B,
- if $y \leq l_1\cos\left(\gamma_A\right) - L\cos\left(\alpha_A\right)$, The ROV is inside area D1 Then, the current value of α and γ can be evaluated using Theorem 2 (3),
- if $y \geq l_1\cos\left(\gamma_A\right) - L\cos\left(\beta_A\right)$, the ROV is inside area D2. Then, the current value of β and γ can be evaluated using Theorem 2 (4).

An additional area F can be defined in presence of horizontal current, corresponding to the area where cables l_2 and l_3 or l_1 and l_3 are crossed, *i.e.* lines associated to $\alpha = \beta$ and $\alpha = \gamma$. The crossing of cables can lead to an entanglement, or simply obstruct the displacement of the buoy on the cable, making the umbilical self-management strategy invalid. Area F must therefore be avoid by the ROV like area C. As illustrated in Figure 10, area F is superposed with the other

areas A, B, C, and D2: area F has priority over the other areas to avoid cables crossing, except area D2 where $l_2 = 0$ and so no entanglement can happen.

There are two boundaries between the areas A and F, the first corresponding to $|\alpha - \beta| = 0$, the second $|\alpha - \gamma| = 0$. To take into account the rigidity of the umbilical and consider a safety margin, area F is evaluated for $|\alpha - \beta| = \theta_{\min}$ and $|\alpha - \gamma| = \theta_{\min}$, where $\theta_{\min} \geq 0$ is the value defined in (50) in Section 5.5.1. Figure 11 illustrates area F for $\theta_{\min} = 10°$.

Following step from [22, Appendix C.2.2], the ROV is inside area F if $y_{area\,F1} \leq y \leq y_{area\,F2}$ where $y_{area\,F1}$ and $y_{area\,F2}$ can be expressed such

$$y_{area\,F1}(x) = \begin{cases} l_1 \cos(\gamma_F) - (L - l_{33}) \cos\left(\psi_{B,x} + \frac{\theta_{\min}}{2} s\right) \\ +l_{33} \cos\left(\psi_{B,x} - \frac{\theta_{\min}}{2} s\right) & \text{if } 0 \leq l_{33} \leq L \\ l & \text{if } l_{33} > L \\ 0 & \text{else,} \end{cases} \tag{67}$$

$$y_{area\,F2}(x) = \begin{cases} l_1 \cos\left(\psi_{P,x} + \frac{\theta_{\min}}{2} s\right) - l_{22} \cos\left(\psi_{P,x} + \frac{\theta_{\min}}{2} s\right) \\ + (L - l_{22}) \cos\left(2\psi_{B,x} - \psi_{P,x} - \frac{\theta_{\min}}{2} s\right) & \text{if } 0 \leq l_{22} \leq L \\ l & \text{if } (l_{22} < 0) \,\&\, (l_{33} \geq L) \\ 0 & \text{else} \end{cases} \tag{68}$$

where γ_F can be evaluated using (65) with $\beta = \psi_{B,x} - \frac{\theta_{\min}}{2} s$, and

$$l_{22} = \frac{l_1 \sin\left(\psi_{P,x} + \frac{\theta_{\min}}{2}\right) + L \sin\left(2\psi_{B,x} - \psi_{P,x} + \frac{\theta_{\min}}{2}\right) - x}{\sin\left(2\psi_{B,x} - \psi_{P,x} + \frac{\theta_{\min}}{2}\right) + \sin\left(\psi_{P,x} - \frac{\theta_{\min}}{2}\right)} \tag{69}$$

$$l_{33} = \frac{x - l_1 \sin(\gamma_{F1}) + L \sin\left(\psi_{B,x} + \frac{\theta_{\min}}{2} s\right)}{\sin\left(\psi_{B,x} + \frac{\theta_{\min}}{2} s\right) + \sin\left(\psi_{B,x} - \frac{\theta_{\min}}{2} s\right)} \tag{70}$$

with $s = \text{sign}(\psi_{B,x})$ if $\psi_{B,x} \neq 0$, $s = -\text{sign}(x)$ else.

Remark if there is no current, *i.e.* $F_{cx,m} = F_{cx,b} = 0$, and $\theta_{\min} > 0$, area F corresponds to $[-x_{\min}, x_{\min}]$, where $x_{\min}$ is evaluated using (49) exposed in Section 5.5.1. Finally, remark area F stops always when it reaches area D2, because no entanglement can be made between l_2 and l_3 or between l_2 and l_1 when $l_2 = 0$.

6.4. Numerical solution of umbilical model

In opposite with the case without current studied in Section 5.3, the strong non-linearity of the relation (65) makes the system (17)-(19) too complex to be solved analytically.

Theorem 3 proposes a numerical solution of system (17)-(19) and values of parameters γ, α, β, l_2 and l_3 inside area A. Let note α_A, β_A,γ_A, l_{2A}, l_{3A} the evaluations of α, β, γ, l_2, l_3 inside area A described in the following theorem.

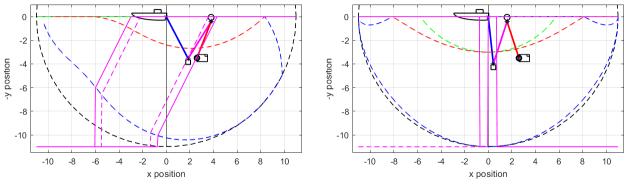

(a) $F_{cx,m} = F_{cx,b} = 0.5F_b$ (b) $F_{cx,m} = F_{cx,b} = 0$

Figure 11: Area F with $\theta_{\min} = 10°$. The plain magenta line corresponds to area F with $\theta_{\min} = 10°$ and the dash magenta line to area F with $\theta_{\min} = 0$.

Theorem 3. *Consider the system (17)-(19) with (x, y) such $|x| \leq l$ and $0 \leq y \leq l$ and suppose (x, y) are inside area A. Considering also the assumption A8 and presence of horizontal current, i.e. (65) and (61). The parameters $\gamma = \gamma_A$ and $l_3 = l_{3A}$ where $\gamma_A \in \left[-\frac{\pi}{2}, \frac{\pi}{2}\right]$ and $l_{3A} \in [0, L]$ are the solutions of the system*

$$\begin{cases} x = l_1 \sin(\gamma_A) - l_2 \sin(\alpha_A) + l_{3A} \sin(\beta_A) \\ y = l_1 \cos(\gamma_A) - l_2 \cos(\alpha_A) + l_{3A} \cos(\beta_A) \end{cases} \tag{71}$$

with

$$\beta_A = \psi_{B,x} + \tag{72}$$

$$atan\left(\frac{\left(2\frac{F_{tm,x}}{F_{tb,x}} - \cos(\Delta\psi_x)\right)\tan(\gamma_A - \psi_{P,x}) - \sin(\Delta\psi_x)}{\cos(\Delta\psi_x) - \tan(\gamma_A - \psi_{P,x})\sin(\Delta\psi_x)}\right) \tag{73}$$

and $l_2 = L - l_{3A}$, $\alpha_A = 2\psi_{B,x} - \beta_A$.

Consider now the system inside area B. Since the buoy reaches the surface, one has $y = l_3 \cos(\beta)$. Due to the current, the umbilical can always be taut, but the relation (61) does not hold because the buoy is not on the ellipse $\mathcal{E}_2$ in this configuration.

Theorem 4 proposes a numerical solution of system (17)-(19) and values of parameters γ, α, β, l_2 and l_3 in all areas.

Theorem 4. *Consider the system (17)-(19) with (x, y) and such $y_{area\,E}(x) > y$, i.e. the configuration is possible. Considering also the Assumption A8 and presence of horizontal current. Let β_A,γ_A and l_{3A} be the value of β, γ and l_3 estimated using Theorem 3 for the couple (x, y). Consider the following cases:*

(1) if $y < y_{area\,C}(x)$, the ROV is inside area C, so the model (17)-(19) is not valid.

(2) if $y < l_{3A} \cos(\beta_A)$, the ROV is inside area B and $\alpha = \alpha_B$, $\beta = \beta_B$, $\gamma = \gamma_B$ where

$$\alpha_B \in \left[-\frac{\pi}{2}, \frac{\pi}{2}\right] \tag{74}$$

$$\beta_B \in \begin{cases} [-\pi, 0] & \text{if } F_{cx} < 0 \\ [0, \pi] & \text{else.} \end{cases} \tag{75}$$

$$\gamma_B \in \begin{cases} \left[\psi_{P,x}, \frac{\pi}{2}\right] & if\ \left(F_{cx} > 0\right) \& (x > 0) \\ \left[-\frac{\pi}{2}, \psi_{P,x}\right] & if\ \left(F_{cx} < 0\right) \& (x < 0) \\ \left[-\frac{\pi}{2}, \frac{\pi}{2}\right] & else. \end{cases} \quad (76)$$

are the solutions of the system

$$\begin{cases} x = l_1 \sin\left(\gamma_B\right) - l_2 \sin\left(\alpha_B\right) + l_3 \sin\left(\beta_B\right) \\ y = l_3 \cos\left(\beta_B\right) \\ 0 = \frac{F_{tb,x}}{F_{tm,x}} \sin\left(\beta_B - \psi_{B,x}\right) \sin\left(\gamma_B - \alpha_B\right) \\ -\sin\left(\gamma_B - \psi_{P,x}\right) \sin\left(\beta_B - \alpha_B\right) \end{cases} \quad (77)$$

with $l_2 = l_1 \frac{\cos(\gamma_B)}{\cos(\alpha_B)}$, $l_3 = L - l_2$.

(3) if $y > l_{3A} \cos\left(\beta_A\right)$ *and* $y \leq l_1 \cos\left(\gamma_A\right) - L \cos\left(\alpha_A\right)$, *the ROV is inside area D1 with* $l_2 = L$, $l_3 = 0$, $\beta = 0$ *and values of* α, γ *can be evaluated using Theorem 2 (3).*

(4) if $y > l_{3A} \cos\left(\beta_A\right)$ *and* $y \geq l_1 \cos\left(\gamma_A\right) - L \cos\left(\beta_A\right)$, *the ROV is inside area D2 with* $l_2 = 0$, $l_3 = L$, $\alpha = 0$ *and values of* β, γ *can be evaluated using Theorem 2 (4).*

(5) else, the ROV is inside area A with $\beta = \beta_A$, $\gamma = \gamma_A$ *and* $l_3 = l_{3A}$, *and other parameters can be evaluated using Theorem 3.*

Remark Theorem 4 is valid inside area F, this area pointing only if the umbilical makes an entanglement or not. If the ROV is inside area F and not inside area D2 simultaneously, it is strongly recommended to leave it by the same side the ROV is entered to avoid entanglement.

6.5. Forces applied on the ROV with current

This section extends results of Section 5.5.2 by considering the presence of currents. Excluding the ROV propulsion, the sum $F_{ROV,x}$ and $F_{ROV,y}$ of the external forces applied on the ROV on axis Ox and Oy can be expressed as

$$\vec{F}_{ROV,x} = \left(-T_3 \sin(\beta) + F_{cx,ROV}\right) \vec{x} \quad (78)$$

$$\vec{F}_{ROV,y} = \left(T_3 \cos(\beta) + F_{cy,ROV}\right) \vec{y} \quad (79)$$

where $F_{cx,ROV}$ and $F_{cy,ROV}$ are the forces of the horizontal and vertical currents applied on the ROV and T_3 has been introduced in Section 6.2.

Following step of [22, Appendix D] the forces $F_{ROV,x}$ and $F_{ROV,y}$ can be expressed as

$$\vec{F}_{ROV,x}.\vec{x} = -\left(F_{tb,x} \frac{\cos\left(2\psi_{B,x} - \beta\right)}{2\cos\left(\beta - \psi_{B,x}\right)} - F_{cx,b}\right) \tan(\beta) + F_{cx,ROV} \quad (80)$$

$$\vec{F}_{ROV,y}.\vec{y} = F_{tb,x} \frac{\cos\left(2\psi_{B,x} - \beta\right)}{2\cos\left(\beta - \psi_{B,x}\right)} - F_{cx,b} + F_{cy,ROV}. \quad (81)$$

7. Umbilical for Sea exploration: 3D case

In this section, the 3-Dimensionnal case with and without presence of horizontal current is studied. This case is more complex and can be solved only using numerical method.

7.1. 3-Dimensionnal case in absence of horizontal current

In absence of horizontal current, the three dimensions case can be simply solved using the two dimensions case. Let define the 3D referential $\mathcal{R}_{3D} = (x, y, z)$ of origin $O = (0, 0, 0)$, where y is the vertical axis oriented to the ground. $(x, 0, z)$ is the horizontal plan at the sea level. $(x, y, 0)$ is the vertical plan such $\vec{OR}.\vec{z} = 0$, where $\vec{OR}$ is the vector between the boat and the ROV. One observes the umbilical is always at the equilibrium inside the plan $P = (\vec{OR}.\vec{x}, y, \vec{OR}.\vec{z})$, so the solution of the 3D case without current is the solution of the 2D-case performed inside P.

7.2. 3-Dimensionnal case with horizontal current: Geometrical model

The 3D case introduces new degrees of freedom, described by parameters defined in the plans $P_{oxy} = (O, x, y)$ and $P_{ozy} = (O, z, y)$. Let γ and ϕ be respectively the angles between the boat and the ballast M in P_{oxy} and P_{ozy}, α and μ be the angles between the ballast and the buoy in P_{oxy} and P_{ozy}, and β and η be the angles between the buoy and the ROV in P_{oxy} and P_{ozy}. The length l_{1x} and l_{1z} are the projections of l_1 on P_{oxy} and P_{ozy}, same for l_{2x}, l_{2z}, l_{3x} and l_{3z}. All these parameters are illustrated in the Figure 12.

In a configuration where the umbilical is taut, and using the coordinates of the ROV, the system can be expressed such

$$x = l_{1x} \sin(\gamma) - l_{2x} \sin(\alpha) + l_{3x} \sin(\beta) \quad (82)$$

$$y = l_{1x} \cos(\gamma) - l_{2x} \cos(\alpha) + l_{3x} \cos(\beta) \quad (83)$$

$$z = l_{1z} \sin(\phi) - l_{2z} \sin(\mu) + l_{3z} \sin(\eta) \quad (84)$$

with

$$l_1^2 = l_{1x}^2 + \sin(\phi)^2\, l_{1z}^2 \quad (85)$$

$$l_2^2 = l_{2x}^2 + \sin(\mu)^2\, l_{2z}^2 \quad (86)$$

$$l_3^2 = l_{3x}^2 + \sin(\eta)^2\, l_{3z}^2 \quad (87)$$

$$L = l_2 + l_3 \quad (88)$$

Let expressed $\left(x_M, y_M, z_M\right)$ the coordinate of the ballast M, $L_x = l_{1x} + l_{2x}$ and $L_z = l_{1z} + l_{2z}$. Since the buoy is still moving freely on the umbilical, its position is on

- the ellipse $\mathcal{E}_2$ of centers M and R with the two radius $\frac{L_x}{2}$ and $\sqrt{\left(\frac{L_z}{2}\right)^2 - \frac{(x-x_M)^2 + (y-y_M)^2}{4}}$ in P_{oxy},
- the ellipse $\mathcal{E}_3$ of centers M and R with the two radius $\frac{L_z}{2}$ and $\sqrt{\left(\frac{L_z}{2}\right)^2 - \frac{(z-z_M)^2 + (y-y_M)^2}{4}}$ in P_{ozy}.

Thus, since the buoy does not touch the surface (not inside area B and C), these properties lead to

$$\alpha = 2\psi_{B,x} - \beta \quad (89)$$

$$\mu = 2\psi_{B,z} - \eta \quad (90)$$

where $\psi_{B,x}$ has been defined in Section 6.1 in P_{oxy} and $\psi_{B,z}$ is the orientation of the force $F_{tb,z}$, similarly to $\psi_{B,x}$ but inside P_{ozy}, which will be described in Section 7.3.

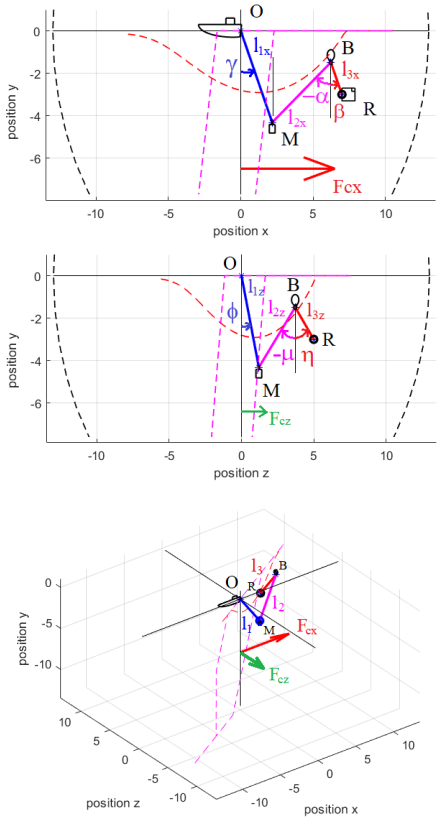

Figure 12: Parameters for Sea Exploration with current in 3D case, for $(x, y, z) = (5, 2.5, 3)$. M: fixed ballast. B: sliding buoys. The blue, magenta, red lines correspond to l_1, l_2, l_3. Black dash line: area where the ROV can move due to the umbilical length. Red and green arrows: horizontal currents F_{cx} and F_{cz} in direction $\vec{O}x$ and $\vec{O}z$ with $F_{cx} = 3F_{cz}$.

7.3. Study of the model

Let $F_{cx,m}$ and $F_{cx,b}$ be the forces of the horizontal current applied on the ballast M and buoy B on the axis $\vec{O}x$, as exposed in Section 6.1. Since they exist only in P_{oxy}, the forces applied on the system in P_{oxy} are similar to the 2D case studied in Section 6.1 and 6.2.

Let $F_{cz,m}$ and $F_{cz,b}$ be the forces of the horizontal current applied on the ballast M and buoy B on the axis $\vec{O}z$ such $F_{cz,m} > 0$ corresponds to a current in the direction $\vec{O}z$, same for $F_{cz,b}$, as illustrated on Figure 12. These ones exist only in P_{ozy}. Let also define the sums of forces $F_{tm,z}$ and $F_{tb,z}$ such

$$F_{tm,z} = \sqrt{P^2 + F_{cz,m}^2} \tag{91}$$

$$F_{tb,z} = \sqrt{F_b^2 + F_{cz,b}^2} \tag{92}$$

with their incidence angles

$$\tan\left(\psi_{P,z}\right) = \frac{F_{cz,m}}{P} \tag{93}$$

$$\tan\left(\psi_{B,z}\right) = -\frac{F_{cz,b}}{F_b}. \tag{94}$$

When the buoy does not touch the surface, the relation (65) linking $F_{tm,x}$, $F_{tb,x}$, γ and β are still valid in the plan P_{oxy}. Following the same steps than in Section 6.1, 6.2 and [22, Appendix C.1], one may write

$$F_{tm,z}\frac{\sin\left(\Phi\right)}{\sin\left(\Phi + H + \Delta\psi_z\right)} = F_{tb,z}\frac{\sin\left(H\right)}{\sin\left(2H\right)} \tag{95}$$

and

$$\tan\left(H\right) = \frac{\left(2\frac{F_{tm,z}}{F_{tb,z}} - \cos\left(\Delta\psi_z\right)\right)\tan\left(\Phi\right) - \sin\left(\Delta\psi_z\right)}{\cos\left(\Delta\psi_z\right) - \tan\left(\Phi\right)\sin\left(\Delta\psi_z\right)} \tag{96}$$

with $\Phi = \phi - \psi_{P,z}$, $H = \eta - \psi_{B,z}$ and $\Delta\psi_z = \psi_{P,z} - \psi_{B,z}$. Note if $F_{cz,m} = F_{cz,b} = 0$, one has $\psi_{P,z} = \psi_{B,z} = 0$, and so (90) is equal to $\mu = -\eta$ and (96) is equal to $\tan\left(\eta\right) = \left(2\frac{F_{tm,z}}{F_{tb,z}} - 1\right)\tan\left(\phi\right)$.

7.4. Numerical solution of umbilical model

The system (82)-(84) have 14 unknown parameters: l_{1x}, l_{1z},l_{2x}, l_{2z}, l_{3x}, l_{3z}, l_2, l_3, α, β, γ, ϕ, μ, η. Enough equations must be found to solve the system, and a small number of variables must be selected to obtain a numerical resolution with a reduced computing time. Using relations found in previous sections and other presented in this section, the Theorem 5 proposes a numerical resolution of system (82)-(84) using only variables γ, ϕ, l_3.

Following steps described in [22, Appendix E.1], one can obtain

$$l_{1x}^2 = \frac{l_1^2}{\left(1 + \tan\left(\phi\right)^2\cos\left(\gamma\right)^2\right)} \tag{97}$$

$$l_{1z}^2 = \frac{l_1^2}{\left(\sin\left(\phi\right)^2 + \left(\frac{\cos(\phi)}{\cos(\gamma)}\right)^2\right)} \tag{98}$$

and the same for l_{2x}, l_{2z} and l_{3x}, l_{3z} replacing l_1, γ, ϕ by l_2, α, μ and l_3, β, η.

Using (97)-(98) and their equivalent for l_{2x}, l_{2z}, l_{3x}, l_{3z}, the system (82)-(84) has now only 8 unknown parameters: l_2, l_3, α, β, γ, ϕ, μ, η. (88) solves $l_2 = L - l_3$ and (89)-(90) express β, η with α, μ, leaving 5 unknown parameters. (65) and (96) provide two other relations to express β, η with γ, ϕ. The system (82)-(84) provide the last three equations, to solve for the variables γ, ϕ, l_3.

Theorem 5. *Consider the system (82)-(84) with (x, y, z) such $|x| \leq l$, $|z| \leq l$ and $0 \leq y \leq l$ not inside the areas B and C. Considering also the assumption A8 and presence of horizontal current. The parameters γ, ϕ, l_3 such*

$$\gamma \in \begin{cases} \left[\psi_{P,x}, \frac{\pi}{2}\right] & \text{if } \left(F_{cx} > 0\right) \& \left(x > 0\right) \\ \left[-\frac{\pi}{2}, \psi_{P,x}\right] & \text{if } \left(F_{cx} < 0\right) \& \left(x < 0\right) \\ \left[-\frac{\pi}{2}, \frac{\pi}{2}\right] & \text{else.} \end{cases} \tag{99}$$

$$\phi \in \begin{cases} \left[\psi_{P,z}, \frac{\pi}{2}\right] & if\ \left(F_{cz} > 0\right) \& \left(z > 0\right) \\ \left[-\frac{\pi}{2}, \psi_{P,z}\right] & if\ \left(F_{cz} < 0\right) \& \left(z < 0\right) \\ \left[-\frac{\pi}{2}, \frac{\pi}{2}\right] & else. \end{cases} \tag{100}$$

$$l_3 \in [0, L] \tag{101}$$

are the solutions of the system

$$\begin{cases} x = l_{1x}\sin(\gamma) - l_{2x}\sin(\alpha) + l_{3x}\sin(\beta) \\ y = l_{1x}\cos(\gamma) - l_{2x}\cos(\alpha) + l_{3x}\cos(\beta) \\ z = l_{1z}\sin(\phi) - l_{2z}\sin(\mu) + l_{3z}\sin(\eta) \end{cases} \tag{102}$$

with

$$\beta = \psi_{B,x} + atan\left(\frac{\left(2\frac{F_{tm,x}}{F_{tb,x}} - \cos\left(\Delta\psi_x\right)\right)\tan\left(\gamma - \psi_{P,x}\right) - \sin\left(\Delta\psi_x\right)}{\cos\left(\Delta\psi_x\right) - \tan\left(\gamma - \psi_{P,x}\right)\sin\left(\Delta\psi\right)}\right) \tag{103}$$

$$\eta = \psi_{B,z} + atan\left(\frac{\left(2\frac{F_{tm,z}}{F_{tb,z}} - \cos\left(\Delta\psi_z\right)\right)\tan\left(\phi - \psi_{P,z}\right) - \sin\left(\Delta\psi_z\right)}{\cos\left(\Delta\psi_z\right) - \tan\left(\phi - \psi_{P,z}\right)\sin\left(\Delta\psi_z\right)}\right) \tag{104}$$

where (α, μ) *are evaluated using (89)-(90),* $l_2 = L - l_3$, $\left(l_{1x}, l_{1z}\right)$ *evaluated using (97)-(98), and* $\left(l_{2x}, l_{2z}\right)$ *and* $\left(l_{3x}, l_{3z}\right)$ *evaluated similarly to* $\left(l_{1x}^2, l_{1z}^2\right)$ *using* l_2, α, μ *and* l_3, β, η.

The Theorem 5 does not consider specific cases for the areas D1 and D2 because these configurations can be solved by taking $l_3 = 0$ or $l_3 = L$ if required. Since the Theorem 5 provides a solution only outside the areas B and C, the following Theorem 6 describes the solution of the system in all cases. Let define l_{3xA} and β_A the evaluation of l_{3x} and β by Theorem 5.

Theorem 6. *Consider the system (82)-(84) with* (x, y, z) *such* $|x| \leq l$, $|z| \leq l$ *and* $0 \leq y \leq l$ *inside area B. Considering also the assumption A8 and presence of horizontal current. If* $y < l_{3xA}\cos\left(\beta_A\right)$, *the ROV is inside area B and* α_B, β_B, γ_B, ϕ_B, μ_B *and* η_B *where*

$$\alpha_B \in \left[-\frac{\pi}{2}, \frac{\pi}{2}\right], \quad \mu_B \in \left[-\frac{\pi}{2}, \frac{\pi}{2}\right] \tag{105}$$

$$\beta_B \in \begin{cases} [-\pi, 0] & if\ F_{cx} < 0 \\ [0, \pi] & else. \end{cases}, \eta \in \begin{cases} [-\pi, 0] & if\ F_{cz} < 0 \\ [0, \pi] & else. \end{cases} \tag{106}$$

$$\gamma_B \in \begin{cases} \left[\psi_{P,x}, \frac{\pi}{2}\right] & if\ \left(F_{cx} > 0\right) \& \left(x > 0\right) \\ \left[-\frac{\pi}{2}, \psi_{P,x}\right] & if\ \left(F_{cx} < 0\right) \& \left(x < 0\right) \\ \left[-\frac{\pi}{2}, \frac{\pi}{2}\right] & else. \end{cases} \tag{107}$$

$$\phi_B \in \begin{cases} \left[\psi_{P,z}, \frac{\pi}{2}\right] & if\ \left(F_{cz} > 0\right) \& \left(z > 0\right) \\ \left[-\frac{\pi}{2}, \psi_{P,z}\right] & if\ \left(F_{cz} < 0\right) \& \left(z < 0\right) \\ \left[-\frac{\pi}{2}, \frac{\pi}{2}\right] & else. \end{cases} \tag{108}$$

are the solutions of the system

$$\begin{cases} x = l_{1x}\sin\left(\gamma_B\right) - l_{2x}\sin\left(\alpha_B\right) + l_{3x}\sin\left(\beta_B\right) \\ z = l_{1z}\sin\left(\phi_B\right) - l_{2z}\sin\left(\mu_B\right) + l_{3z}\sin\left(\eta_B\right) \\ 0 = l_{2x}cos(\alpha_B) - l_{1x}cos(\gamma_B) \\ 0 = l_{2z}cos(\mu_B) - l_{1z}cos(\phi_B) \\ 0 = \frac{F_{tb,x}}{F_{tm,x}}\sin\left(\beta_B - \psi_{B,x}\right)\sin\left(\gamma_B - \alpha_B\right) \\ -\sin\left(\gamma_B - \psi_{P,x}\right)\sin\left(\beta_B - \alpha_B\right) \\ 0 = \frac{F_{tb,z}}{F_{tm,z}}\sin\left(\eta_B - \psi_{B,z}\right)\sin\left(\phi_B - \mu_B\right) \\ -\sin\left(\phi_B - \psi_{P,z}\right)\sin\left(\eta_B - \mu_B\right) \end{cases} \tag{109}$$

where $l_{3x} = \frac{y}{\cos(\beta_B)}$, $l_{3z} = \frac{y}{\cos(\eta_B)}$, $l_3 = \sqrt{l_{3x}^2 + l_{3z}^2}$, $l_2 = L - l_3$, $\left(l_{1x}, l_{1z}\right)$ *evaluated using (97)-(98), and* $\left(l_{2x}, l_{2z}\right)$ *evaluated similarly to* $\left(l_{1x}^2, l_{1z}^2\right)$ *using* l_2, α, μ.

7.5. Evaluation of the areas in 3D

To evaluate the areas in 3D case in presence of horizontal current, numerical approaches similar to those from [22, Section 6.3] can be used. However, in order to obtain a fast computation, approximations of the areas B, C, F are proposed here. These approximate areas are sufficient requirements to guarantee the umbilical is taut and absence of entanglement. Areas D1 and D2 are not studied because useless for Theorems 5 and 6 and the control of the ROV. Area E is of course unchanged.

Let $F_{c,m} = \sqrt{F_{cx,m}^2 + F_{cz,m}^2}$ and $F_{c,b} = \sqrt{F_{cx,b}^2 + F_{cz,b}^2}$ be the sum of the horizontal currents applied on the ballast and the buoy, associated to orientations $\zeta_m = \text{atan}\left(\frac{F_{cz,m}}{F_{cx,m}}\right)$ and $\zeta_b = \text{atan}\left(\frac{F_{cz,b}}{F_{cx,b}}\right)$. Let define also $\varepsilon = \text{atan}\left(\frac{z}{x}\right)$ the orientation of the ROV projected on the plan (O, x, z).

The lengths $\mathcal{L}_{xz} = \left\{l_{1x}, l_{1z}, l_{2x}, l_{2z}, l_{3x}, l_{3z}\right\}$ are respectively smallest or equal to l_1, l_2 and l_3. When $\varepsilon = \zeta_m = \zeta_b$, the 3D case can be assimilated to a 2D case in the plan $\left(O, \vec{OR}, \vec{Oy}\right)$ with $F_{c,m}$ and $F_{c,b}$ as horizontal currents. In the same way, when $\cos\left(\varepsilon - \zeta_m\right) = \cos\left(\varepsilon - \zeta_b\right) = 0$, the horizontal currents push the ballast upward and the sliding buoy downward perpendicularly to the plan, reducing values of $\mathcal{L}_{xy}$ without influencing their position in the direction $\vec{OR}$: the 3D case can so be assimilated to a 2D case in the plan $(O, \vec{OR}, \vec{Oy})$ without horizontal current and with shorter lengths l_1, l_2 and l_3.

Considering previous points, 3D areas B, C and F can so be upper-bounded by $y_{area\ B}$, $y_{area\ F1}$ and $y_{area\ F2}$ exposed in Section 6.3 by replacing x by $d = \sqrt{x^2 + y^2}$, and replacing

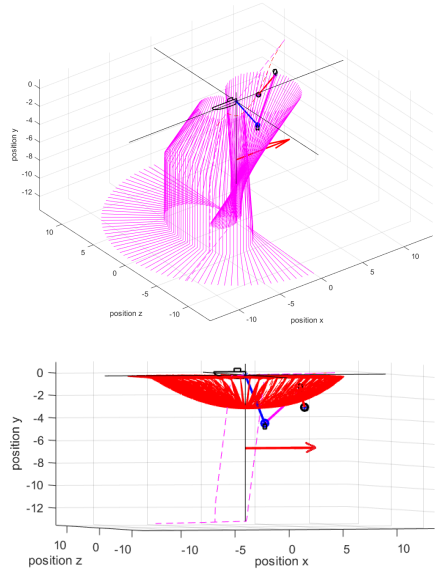

Figure 13: Approximate areas F (magenta) and B (red) in the 3D case.. The red arrow: horizontal current $F_{c,m} = F_{c,b}$

$F_{cx,m}$ and $F_{cx,b}$ by $\bar{F}_{cx,m}$ and $\bar{F}_{cx,b}$ such

$$\bar{F}_{cx,m} = F_{c,m} \cos\left(\varepsilon - \zeta_m\right) \tag{110}$$

$$\bar{F}_{cx,b} = F_{c,b} \cos\left(\varepsilon - \zeta_b\right). \tag{111}$$

These boundaries provide sufficient requirements for the umbilical to stay taut outside this area B and F without entanglement. One can observe area F should theoretically exist only in the plane $\mathcal{P}$ where $\varepsilon = \zeta_m = \zeta_b$, else the projections of cables l_1, l_2 and l_3 are crossed on $\left(O, \vec{OR}, \vec{Oy}\right)$ but not the true cables in the three dimensional space. However, the ROV must bypass area F to not make an entanglement when it wants to cross the plane $\mathcal{P}$ (ex: if $\mathcal{P}$ is the plan (O, x, y), an entanglement is possible if the ROV takes the shortest pass from coordinate $z = 1$ to $z = -1$). The area created by the boundaries $\bar{y}_{area\,F1}$ and $\bar{y}_{area\,F2}$ allows to bypass area F softly without risk of entanglement, as illustrated in Figure 13.

8. Umbilical for diving exploration in presence of large obstacles

In the strategy exposed in previous sections, the presence of obstacles higher than the minimum seafloor level is not considered. The operator must watch the model of the umbilical and its knowledge of the environment to check if the position of the umbilical does not coincide with the presence of an obstacle. In presence of large/high obstacles on the seafloor, the angles performed by the umbilical can be very restrictive for the navigation and lead to a contact between the umbilical and an obstacle, specifically when the ROV is far from the boat, see Figure 14.

A strategy described in [22] can be defined, where the umbilical stays close to the vertical behind the ROV in all

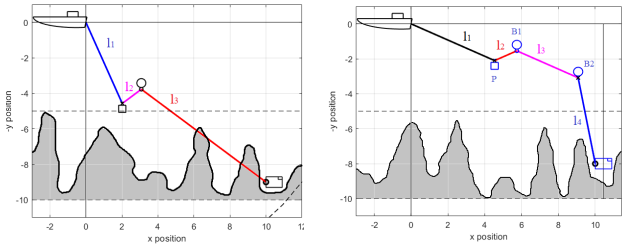

(a) Sea exploration strategy (b) Diving exploration strategy

Figure 14: Comparison between methods exposed in Section 5 and 8. For the same exploration area $[0, 10]\times[5, 10]$, the diving exploration strategy allows to keep the cable l_4 close to the vertical and so avoid contact with obstacle.

situations, since it stays inside a defined area. This strategy allows to dive vertically without risk of collision between the umbilical and a possible obstacle.

9. Umbilical in presence of waves

9.1. Wave model

In presence of waves, the position $O = \left(0, y_0\right)$ of the boat can be modeled as

$$y_0(t) = -\cos\left(\frac{t}{T}\right)\frac{h_w}{2}$$

where $T = \frac{t_w}{2\pi}$, with t_w the time period of the waves, h_w the wave's height, and $t = 0$ corresponds to the time of the wave's highest position. Since the axis y is oriented to the seafloor, the highest position of the wave corresponds to $y_0 = -\frac{h_w}{2}$. The velocity and the acceleration of the waves can be expressed as

$$\dot{y}_0(t) = \sin\left(\frac{t}{T}\right)\frac{h_w}{2T} \tag{112}$$

$$\ddot{y}_0(t) = \cos\left(\frac{t}{T}\right)\frac{h_w}{2T^2}, \tag{113}$$

and their maximum values are respectively $v_{w,\max} = \frac{h_w}{2T}$ and $a_{w,\max} = a_w(0) = \frac{h_w}{2T^2}$.

The influence of waves is maximum at the surface and decreases with depth, to become negligible. Since the cable l_1 links the ballast and the boat, the ballast is directly influenced by the waves. When a wave rises, the cable is kept taut because the action of wave and ballast are opposite. When a wave falls, the cable stays stretched only if the ballast have a weight allowing it to accelerate and fall faster than the wave. A condition on the ballast's mass to guarantee that the cable stays taut is defined in Section 9.2.

When the ROV and the buoy stay deep under the surface, the direct influence of wave on them can be neglected or expressed inside the term $F_{cy,m}$, already considered in previous sections. However, the buoy receives an indirect influence from the ballast movement, which follows an amplitude proportional to the wave's height. When the ballast falls, the

cable can stay stretched between the ballast and the buoy because their actions are opposite. When the ballast rises, the cable l_2 is loosen between the ballast and the buoy, which is like drop freely in the water. If the ballast is chosen such as it falls at the same velocity than the waves, the cable l_2 will stay stretched only if the buoy can rise faster than the wave's rising. A condition on the buoy's volume to guarantee the cable stays taut is defined in Section 9.3.

If the conditions on the ballast and buoy to guarantee that the umbilical stays taut even in presence of waves are respected, the models studied in previous sections are still valid in quasi-static equilibrium and can be evaluated considering $\bar{y} = y - y_0(t)$ instead of y in calculations, and by extending the boundary $y_{area\,C}$ of area C to $\bar{y}_{area\,C} = y_{area\,C} + h_w$ to guarantee that the buoy will not reach the surface and so be directly affected by the waves.

9.2. Study of the ballast's fall

9.2.1. Ballast's fall velocity

When the umbilical is not taut between the boat and the ballast, the ballast falls with only the drag force and the action of the cable l_2 to slow it. Consider the drag force $\vec{F}_{fm} = -K_m v_m^2 \frac{\vec{v}_m}{\|\vec{v}_m\|}$, where v_m is the ballast's velocity, with $\vec{v}_m = v_{m,x}\vec{x} + v_{m,y}\vec{y}$ and $v_m = \sqrt{v_{m,x}^2 + v_{m,y}^2}$, $K_m = \frac{1}{2}\rho_{water} S_m C_x$, where S_m is the surface of the ballast and C_x is the drag coefficient ($C_x = 0.47$ for a spherical ballast). Let m_m, ρ_m and a_m be respectively the mass, the volumetric mass and the vertical acceleration of the ballast. To find the weight of the ballast which can compensate the wave's action in all situations, we consider the worst case, where $\vec{T}_2 = -F_b\vec{y}$, *i.e.* the maximum force that the buoy can exert on the ballast.

Finally, we suppose here that the umbilical is sinking, so its influence is not a constraint for the ballast's fall and its drag force can be neglected or considered to be included in the drag force of the ballast. However, the ballast must counter the inertia of the umbilical, so the mass m_c of the cable l_1 is added to the inertia of the ballast.

By performing the Fundamental Principle of Dynamics (FPD) on the axis y, as exposed in [22, Appendix I.1], one gets the relation between the velocity and the acceleration of the ballast during its fall:

$$\left(m_m + m_c\right)\dot{v}_{m,y} = B - K_m v_{m,y}^2 \tag{114}$$

with $B = m_m g - \left(\rho_{water} V_m g + F_{cy,m} + F_b\right)$. Due to the form of the solution of (114), $v_{m,y}$ and $a_{m,y}$ are respectively increasing and decreasing because of the equilibrium, and one has $v_{m,y,\max} = v_{m,y,eq}$ and $a_{m,y,\max} = a_{m,y}(0)$, respectively the maximum velocity and acceleration of the ballast.

9.2.2. Choice of ballast's weight

To counter-balance the waves effect, one must have $v_{m,y,\max} > v_{w,\max}$ and $a_{m,y}(0) > a_w(0)$. According to the proofs described in [22, Appendix I.1], these conditions are respected if m_m is chosen such that:

$$m_m > \max\left(\left[m_1, m_2\right]\right) \tag{115}$$

with

$$m_1 = \frac{K_m}{g}\left(\frac{h_w}{2T}\right)^2 + \frac{\left(\rho_{water} V_m g + F_{cy,m} + F_b\right)}{g} \tag{116}$$

$$m_2 = \frac{\left(\rho_{water} V_m g + F_{cy,m} + F_b + m_c \frac{h_w}{2T^2}\right)}{g - \frac{h_w}{2T^2}}. \tag{117}$$

Remark: if $\frac{h_w}{2T^2} > g$, the wave falls too fast for the ballast to keep the umbilical taut.

Example 1. *Consider a classic swell of time period $t_w = 8s$ and height $h_w = 1m$ and suppose that there is no vertical current, so i.e. $F_{cy,m} = 0$. Consider a spherical ballast of radius $R_m = 0.025m$, thus $S_m = 4\pi R_m^2$ and $V_m = \frac{4}{3}\pi R_m^3$ with $C_x = 0.47$. Finally, choose a buoy of force $F_b = 1.275N$, i.e. which can lift a mass of $0.130kg$, an umbilical of mass $m_c = 0.1kg$. Take $g = 9,81m/s$. Using (115), one finds $m_m > 0.2245kg$ with $\rho_m = \frac{m_m}{V_m} = 3430kg/m^3$. These conditions can be respected for a sphere of volume V_m made in cast iron ($\rho_m = 6800kg/m^3$), iron ($\rho_m = 7800kg/m^3$) or lead ($\rho_m = 11350kg/m^3$). For a waves of time period $t_w = 4s$ and height $h_w = 1m$ for the same other conditions, one gets $m_m > 0.3115kg$ with $\rho_m = \frac{m_m}{V_m} = 4759kg/m^3$.*

Note that the ballast's weight must also respect Assumption A1, and can thus be chosen heavier than (115) to guarantee A1, and can be evaluated depending on the buoy's force, which can also be affected by the waves, as described in the next.

9.3. Study of the buoy's rise

9.3.1. Buoy's rise velocity

When the umbilical is not taut between the ballast and buoy, the buoy is like dropped freely in the water. Consider the drag force $\vec{F}_{fb} = -K_b v_b^2 \frac{\vec{v}_b}{\|\vec{v}_b\|}$, where v_b is the buoy velocity with $\vec{v}_b = v_{b,x}\vec{x} + v_{b,y}\vec{y}$ and $v_b = \sqrt{v_{b,x}^2 + v_{b,y}^2}$, and $K_b = \frac{1}{2}\rho_{water} S_b C_x$ where S_b is the surface of the buoy. Let m_b and a_b be the mass and the vertical acceleration of the buoy. In opposite with the ballast case, since the umbilical is loosen, the buoy is not counter-balanced by the ballast or the ROV to counter-balance. However, to satisfy assumption A1, let's introduce a force F_{cable} to design the buoy and so to guarantee that the action of the buoy is strong enough (example : $F_{cable} = m_{cL} g$, with m_{c2} the mass of the cable L in water).

By performing the FPD on axis y, as exposed in [22, Appendix I.2], one gets the relation between the velocity and acceleration of the ballast:

$$-m_b \dot{v}_{b,y} = B_b + K_b v_{b,y}^2 \tag{118}$$

with $B_b = m_b g + F_{cable} - \left(\rho_{water} V_b g + F_{cy,m}\right)$. Consider here that the mass m_b can be approximated by $m_b = k_b \rho_{water} V_b$, with $0 < k_b < 1$ a ratio between the Archimedes' force and the weight of the buoy, for example $k_b = 0.1$. Thus, one can

also express B_b such as $B_b = -\left(1-k_b\right)\rho_{water}V_b g - F_{cy,m} + F_{cable}$.

When the cable is loosen, the vertical velocity of the buoy at the equilibrium can be expressed as

$$v_{b,y,eq} = \sqrt{\frac{1}{K_b}\left(\rho_{water}V_b g + F_{cy,m} - \left(m_b g + F_{cable}\right)\right)} \quad (119)$$

and its acceleration at time $t = 0$ is:

$$a_{b,y}(0) = \frac{1}{m_b}\left(\left(\rho_{water}V_b g + F_{cy,m}\right) - \left(m_b g + F_{cable}\right)\right). \quad (120)$$

Due to the form of the solution of (118), one has $v_{b,y,\max} = v_{b,y,eq}$ and $a_{b,y,\max} = a_{b,y}(0)$, respectively the maximum velocity and acceleration of the buoy.

9.3.2. Choice of buoy's volume

To counter-balance the waves' effect, one must have

$$v_{b,y,\max} > v_{w,\max} \quad (121)$$

$$a_{b,y}(0) > a_w(0). \quad (122)$$

Following proofs described in [22, Appendix I.2], these conditions are respected if V_b is chosen such as:

$$V_b > \max\left(\left[V_{b1}, V_{b2}\right]\right) \quad (123)$$

where:

$$V_{b1} = \frac{K_b\left(\frac{h_w}{2T}\right)^2 - F_{cy,b} + F_{cable}}{\left(1-k_b\right)\rho_{water}g} \quad (124)$$

$$V_{b2} = \frac{F_{cable} - F_{cy,m}}{\left[\left(1-k_b\right)\rho_{water}g - \frac{h_w}{2T^2}k_b\rho_{water}\right]}. \quad (125)$$

From (125), it can be deduced that if $\frac{\rho_{water}-\rho_{air}}{\rho_{air}}g < \frac{h_w}{2T^2}$, the waves are too fast to be compensated by the buoy and the umbilical cannot be taut. When the buoy is spherical, one can express (124) as $V_{b1} = \frac{4}{3}\pi R_{b1}^3$, with $R_{b1} > X$, where X is the smallest real positive solution of $aX^3 + bX^2 + c = 0$ with $a = -\frac{4}{3}\pi$, $b = \frac{2C_x\pi\left(\frac{h_w}{2T}\right)^2}{(1-k_b)g}$ and $c = \frac{F_{cy,b}+F_{cable}}{(1-k_b)\rho_{water}g}$.

Example 2. *Consider a swell of time period $t_w = 8s$ and height $h_w = 1m$. In this example, we suppose that there is no vertical current and that the buoy is deep enough to be away from the waves' direct influence, i.e. $F_{cy,m} = 0$. Consider a spherical buoy with a drag coefficient $C_x = 0.47$, an umbilical of mass $m_c = 0.1kg$, and take $F_{cable} = m_c g$ and $k_b = 0.1$. Using (123), one gets $V_b = 0.173 \times 10^{-3}m^3 = 0.173L$ and so $F_b = 1.52kg$. From F_b and the results of Section 9.2 for the same parameters as in Example 1, one gets a ballast of mass $m_m = 0.25kg$ with $\rho_m = 3817kg/m^3$. For waves of time period $t_w = 4s$ and height $h_w = 1m$, under the same other conditions, one gets $V_b = 0.789L$, $F_b = 6.97N$, $m_m = 0.9kg$ and $\rho_m = 13776kg/m^3$.*

10. Quasi-static equilibrium: ROV control

The systems presented in previous sections are studied at the equilibrium. However, each time the ROV moves down, up or back, a part of the umbilical becomes temporary loosen. Since a loosen cable can lead to an entanglement and can be complex and/or heavy to compute, an alternative approach is proposed here by controlling the ROV to shorten the transitory phases and to decrease the discrepancy between the models studied and the reality. Thus, the ROV is controlled to move slower than the fall of the ballast and/or the rise of the buoy. As long as their behaviors are faster than the ROV's velocity, the umbilical stays globally taut.

10.1. Main idea and hypotheses

For this work, the ROV never makes a complete turn on itself and goes backwards to come closer to the position $x = 0$: this assumption reduces the stress inside the umbilical and avoids the entanglement. The methodology developed below is dedicated to the sea exploration strategy developed in Section 5, 6 and 7, but it is also valid for the diving exploration strategy developed in Section 8, and can easily be adapted for surface exploration in Section 4 by replacing the sliding buoy by a sliding ballast.

The three behaviors illustrated in Figure 15 can be observed. When the ROV moves forward, the umbilical is always taut because 1) its displacement is in opposition with the force created by the ballast, 2) the ellipse created by the system ballast/buoy/ROV becomes flatter, so the force exerted by the buoy is also opposed to the cable's displacement. During the ascent of the ROV or while it is moving backwards, the umbilical is temporarily loosen between the buoy and the ROV, because the movement gives slack to the buoy. Finally, during the ROV's descent, the umbilical is temporarily loosen between the ballast and the buoy because the ballast and the ROV pull in the same direction while the buoy pulls in the opposite direction, keeping umbilical stretched.

When the displacement of the ROV slackens the umbilical, the fall of the ballast and the ascent of the buoy try to retighten it. However, the fall of the ballast is constrained by the cable l_1, making its displacement similar to a pendulum attached to the boat. On its side, the buoy is as if released freely in the water when the umbilical is not taut, only submitted to its weight and Archimedes' force. Since the displacement of the ballast is limited when it is close to the vertical position, and so is its influence to retighten the umbilical, the control of the ROV will be performed as if the buoy was the only force able to stretch the umbilical during the transition period. This hypothesis can only be taken when the ROV is not inside areas B or C, *i.e.* when the buoy does not touch the surface. Otherwise, the umbilical is stretched by the ballast since $\gamma \neq \psi_{P,x}$ ($\psi_{P,x} = 0$ when there is no current). Since a buoy on the surface can be subject to other forces like wind or waves, one should better avoid working inside area B in practice.

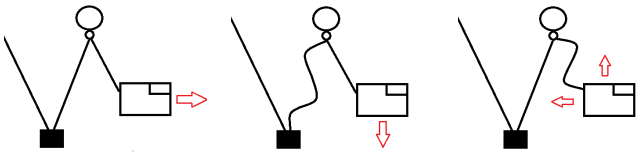

(a) Move forward (b) Moves down (c) Moves up

Figure 15: The umbilical is temporarily loosen when the ROV dives, moves up to surface or backs off. The umbilical is always taut when the ROV moves straight ahead.

Thus, when the ROV rises, dives or goes back, its velocity and acceleration must be bounded by buoy's velocity and acceleration, as defined in the following Section 10.2.

10.2. Maximum ROV velocity and acceleration

Following the same steps as the ones described in Section 9 for the waves, one gets the maximal vertical velocity of the buoy inside the plan (O, x, y)

$$v_{b,y,\max} = \sqrt{\frac{1}{K_b}\left(\rho_{water} V_b g + F_{cy,m} - \left(m_b g + F_{cable}\right)\right)} \tag{126}$$

$$a_{b,y,\max} = \frac{1}{m_b}\left(\left(\rho_{water} V_b g + F_{cy,m}\right) - \left(m_b g + F_{cable}\right)\right) \tag{127}$$

Thus, when the ROV moves up, dives or goes back inside the plan (O, x, y), its velocity and acceleration must be bounded by $v_{b,y,\max}$ and $a_{b,y,\max}$. Note that, since the ROV usually moves slowly when it explores the seafloor or a surface, these conditions are not very restrictive.

If $F_{cy,b}$ is unknown with $F_{cy,b} > 0$, (126)-(127) can be lower bounded by taking $F_{cx,b} = 0$ or a known lower bound of $F_{cx,b}$, and so will be the velocity and acceleration of the ROV. If $F_{cy,b} < 0$, an upper bound of $\left|F_{cy,b}\right|$ must be known to guarantee that $\left(\rho_{water} V_{buoy,i} - m_{buoy,i}\right) g + F_{cy,b} > 0$ (Assumption A6): this upper bound can be used inside (126)-(127). It is recommended to take F_b such that $\left(\rho_{water} V_b - m_b\right) g > \frac{-F_{cy,b}}{2}$ in practice.

During a displacement perpendicular to the plan (O, x, y), *i.e.* along axis $\vec{z}$, the umbilical stays taut for the same conditions since the ROV moves slower than $v_{b,y,\max}$. However, this does not guarantee that the proposed model corresponds to the real umbilical. Indeed, the buoy and the ballast can take time before being realigned into a new plan (O, x, y), because the displacement is not oriented along the same direction as the force exerted by the buoy on the cable. Performing a very simplified FPD on axis $\vec{z}$, the velocity of the buoy can be approximated, in the worst case, by $v_{b,z,\max} = \sqrt{\frac{F_b \Delta z}{L}}$, where Δz is a small displacement of the ROV. Remark that $v_{b,z,\max}$ can be very small when the cable L is long. Since respecting $v_{b,z,\max}$ on axis $\vec{z}$ can be a restrictive condition, a dynamic modelling of the umbilical will be considered in future works.

11. Reversed and transferred models

In the previous section, a model to inspect ship hulls, seafloors or rocky seafloors have been proposed. However, there exist some configurations where it is the surface which is hilly, under the ice or in caves for example. There exist also configurations where the seafloor is very deep, and so the length l_1 is too long to be approximated by a straight line. To solve these problems and to explore new environments, the previous models can be "reversed" or "transferred".

In reversed model, an anchor is used as origin instead of the boat, and ballasts are replaced by buoys and opposite, as illustrated in Figure 16 (a) and (c). The same models can be used, changing the buoyancy of the buoys by the ballasts' weight and opposite. The y axis is also reversed, such that $\vec{Oy}$ axis points to the surface, $y = 0$ corresponds to the depth of the anchor y_{anchor}, and $y_1 < y_2$, means that y_1 is deeper than y_2.

In transferred models, the origin O is translated deeper using an anchor at the end of a cable l_0, not in contact with the seafloor, as illustrated in Figure 16 (b). The anchor becomes the new origin, like the boat was before. The main advantage of this technique is that the cable l_0 linking the anchor to the boat takes all the cable strain due to its length, while cables l_1, l_2 and l_3 can still respect Assumptions A1-A7. Surface exploration and diving exploration strategies can easily be transferred by evaluating the system for $y - l_0$ and by adding the distance l_0 to the result. In the case of the Sea Exploration configuration, the areas are impacted and must be redefined. Areas D1, D2, E and F must be lower than the value of l_0, *i.e.* for $U \in \{D1, D2, E, F\}$ $y_{area\,U} = y_{area\,U} + l_0$. Cases of areas B and C are more complex. If $L < l_1$, area C is also lower than the value of l_0 (and area B still does not exist). If $L > l_1$ and $L - l_1 > l_0$ areas B and C must be elevated of l_0, *i.e.* $y_{area\,U} = y_{area\,U} - l_0$ for $U \in \{B, C\}$, because there is more "space" until the buoy reaches the surface. Else if $l_0 \geq L - l_1$, the buoy cannot reach the surface without loosing cable l_0 or l_1, so area B does not exist and area C can be assimilate to a roof at level $y_{area\,C} = l_0 + l_1 - L$.

In all situations, the anchor must be chosen heavy enough to make the forces exerted by the ballasts, the buoys and the ROV, as well as the currents negligible compared to it.

12. Practical case and experimental results

This section discusses the validity of the assumptions made in the paper, exposes some problems in practical cases and provides some experimental results to illustrate the validity of the study.

12.1. Validity of assumptions taken and choice of ballast and buoy

Consider first the assumptions made in this study. The Assumptions A1, A4, A5, A6 and A8 can easily be respected

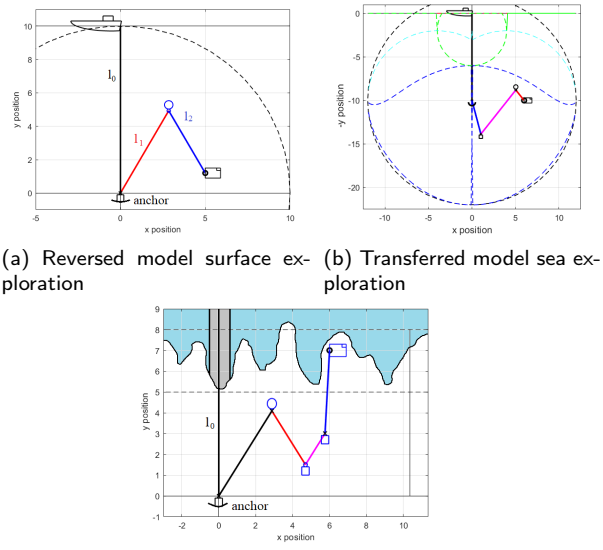

(a) Reversed model surface exploration (b) Transferred model sea exploration

(c) Reversed model diving exploration

Figure 16: Examples of reversed model and transferred model. An anchor is used as origin instead of the boat. Ballasts and buoys are reversed in the reversed models.

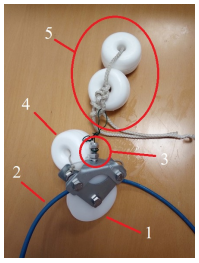

Figure 17: Pulley to obtain a sliding buoy. 1: pulley. 2: umbilical. 3: ball joint to reduce twist effort between the buoy and the pulley. 4: additional buoy and ballast to give a neutral buoyancy to the pulley assembly (without considering the buoys in 5). 5: buoys F_b for the self-management strategy.

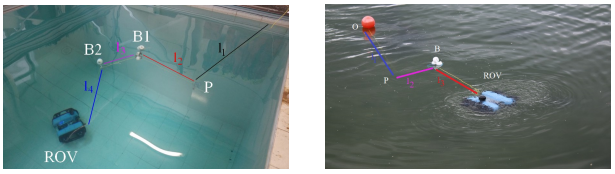

(a) BlueROV during test in pool. Umbilical for diving exploration with presence of large obstacles. $P = 80$g, $F_{b1} = 80$g, $F_{b2} = 280$g, $l_1 = l_4 = L = 1.5$m, so $\eta_{\max} = 10°$.

(b) BlueROV during test at sea. Umbilical for sea exploration, the boat is replaced here by the orange buoy. $P = 255$g, $F_b = 135$g, $l_1 = 2.5$m and $L = 3.5$m.

Figure 18: Materials for experimental tests in pool and sea.

by the choice of the ballast's mass and the buoy's volume. However, Assumptions A2 and A3 can be satisfied only when the umbilical is short enough (50m or less between each points). In case of deep dives where cable l_1 is too long to respect these assumptions, the problem can be solved using the transferred model exposed in Section 11: the additional cable l_0 takes all the cable deformation due to its length, while cables l_1, l_2 and l_3 can respect A2 and A3.

Assumption A7 considers that the friction between the umbilical and the sliding ballast/buoy is quite negligible to allow the ballast/buoy to reach its theoretical equilibrium position. A pulley has been used in practice to let the buoy slide with little friction, as illustrated in Figure 17. Other tests have been performed using karabiner or ring, but the performances obtained are insufficient to correspond to the theory, because of a too strong friction making the equilibrium position strongly dependent of the starting position. Tests show that Assumption A7 can be mostly respected, but cannot be taken neglected, see next section. Note that the radius of the pulley R_p must be taken larger than the radius created by cable's rigidity, involving to take $R_{curve} = R_p$ and so the value of angles $\theta_{\min}$ and $x_{\min}$ exposed in Section 5.5.1. The pulley shown in Figure 17 has been produced to respect perfectly the diameter of our umbilical, but first tests performed using commercial pulleys provided also very good results: the method can so be easily adapted for all kinds of umbilicals. The buoy is linked to the pulley by a mechanical ball joint to avoid twist torque on the umbilical because of the buoy.

The choice of the ballast and buoy can be more complex. First, a ratio $\frac{P}{F_b}$ must be chosen such 1) Assumption A8 is respected, 2) P and F_b are taken such as the umbilical's weight/buoyancy is negligible compared to it and can be deformed by them, 3) the waves are considered. The biggest P and F_b are, the fastest the dynamics of the system is but the strongest the force applied on the ROV by the umbilical is too: the choice of the ballast and buoy is a trade-off between disturbances on the ROV, its maximum velocity and the cable's parameters.

12.2. Materials and experimentation

As illustrated in Figure 18 for the sea exploration and diving exploration, the three configurations have been tested in pool and at sea, in absence of current. To allow accurate measures, the results exposed in this section have been performed in a pool of size $3m \times 4m$, with a depth of $3m$, for the sea exploration strategy, but similar conclusions can be taken for the two others strategies. To obtain a configuration during the measurements, the ROV has been replaced by an anchor immersed at a controlled distance and depth from the origin $(0, 0)$. Let us however call it "ROV" in the text below. The measurements have been made with a measuring tape.

The force exerted by a buoy is evaluated in grams, corresponding to the maximum mass it can lift. One takes $P = 255$g and $F_b = 135$g. The umbilical is floating with the following parameters: diameter 4mm, $R_{curve} = 18$mm. One takes the lengths $l_1 = 2.5$m and $L = 3.5$m. The mass for 6m of umbilical is 85g. The pulley has an internal radius of $R_p = 20$mm.

Let us define E_B, the discrepancy between the measured position $(x_{B,m}, y_{B,m})$ and its theoretical position $(x_{B,th}, y_{B,th})$

of the buoy B for a ROV position (x_{ROV}, y_{ROV}) such as:

$$E_B(x_{ROV}, y_{ROV}) = \sqrt{(x_{B,th} - x_{B,m})^2 + (y_{B,th} - y_{B,m})^2}. \quad (128)$$

Since the movements of the buoy are larger than the ones of the ballast, the accuracy of the method is studied using E_B.

The Figure 19 (a) shows the difference between the measured and theoretical areas B and C. One can observe both results are similar. The most discrepancies between the measured and theoretical areas are mostly due to the measurement error. Indeed, the boundary between areas B and C, *i.e.* the beginning of the umbilical release, is not always simple to observe in practice. During our experiments, the boundary has been measured when the ballast reaches its resting position $(0, l_1)$ or when the umbilical starts to twist due to the lack of tension between the ballast and the buoy. Remind that the height of the buoy (element 5 in Figure 17) must be taking into account in the evaluation of areas B and C.

The Figure 20 illustrates two examples of the difference between theory and practice, and Figure 19 (b) shows the discrepancy E_B for several positions (x_{ROV}, y_{ROV}). These figures show that the discrepancy between the theoretical model and the experimental results is small when the ROV is close to the origin and becomes larger when it moves always. The first reason of this discrepancy is the difference between the angles α, β, γ of the model and the curves performed by the umbilical in practice. Moreover, tests show that the frictions cannot be totally neglected, and so the stabilization of the buoy's position is not always identical depending on the buoy's starting point and the movement performed by the ROV. Results exposed in Figure 19 (b) are so the mean of three measurements. The maximum error measured before averaging was 0.38m for $(x_{ROV}, y_{ROV}) = (3.5\text{m}, 2\text{m})$. Note that this problem of friction is proportional to the horizontality of the cable, and so is negligible when the ROV is close to the origin and increases with the distance, like the discrepancy. Moreover, since the problem of friction slows down the buoy when it approaches its equilibrium position, the measured error is probably independent of the cable's length, making the relative error smaller for longer cable, even if tests would be required to confirm this hypothesis.

Despite the gap between theory and practice, the umbilical remained perfectly taut during all the tests, since the ROV was outside area C, even during the transition phases, and its shape was predictable with a margin error. Note also that the ballast and the buoy used were small, inducing small forces on the cable. Finally, the hypothesis of quasi-static equilibrium has been tested and confirmed: since anchor respected the maximum velocity defined in Section 10.2, when the anchor was moved, the buoy was moving simultaneously, and it stopped moving as soon as the anchor was kept static.

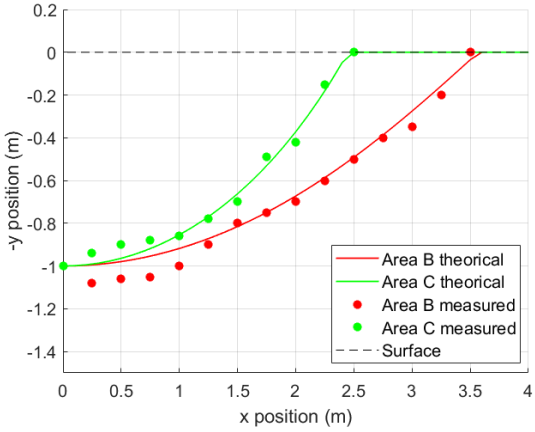

(a) Areas B and C. Plain lines: theoretical areas. Dots: experimental measurements.

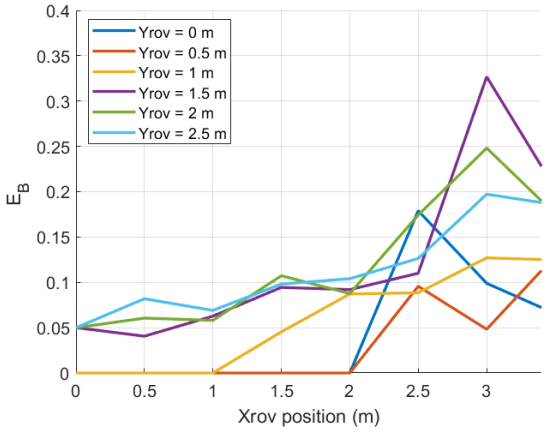

(b) Error E_B

Figure 19: Experimental discrepancy E_B and areas B and C. Each point is the mean of three measurements for the same position (x_{ROV}, y_{ROV}).

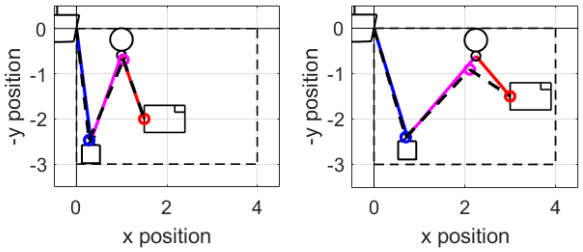

Figure 20: Comparison between theoretical umbilical (colored plain lines) and measured umbilical (large dash black lines). Small black dash lines: poolside. Left: $E_B = 0.107$m. Right: $E_b = 0.327$m, largest discrepancy of the experiment.

12.3. Other practical problems

To perform the model of the umbilical in real time, this work assumes that the position of the ROV is known. To obtain this position, one can use an Ultra Short Baseline (USBL). In absence of USBL, the vertical position y of the ROV can be found using a depth sensor, and the distance d between the ROV and the boat can be found using a sonar, for example.

Another practical problem is the knowledge of the horizontal current F_{cx}, required for the model or the areas' eval-

uation. Since F_{cx} is in the most case unknown, the areas can be defined for two cases: absence of current, *i.e.* $F_{cx} = 0$, and the maximum current $F_{cx,\max}$ against which the ROV will not be able to go upstream, and so the navigation of the ROV is impossible in these conditions. Area B must be evaluated considering $F_{cx} = 0$, and area F must be evaluated considering $F_{cx,\max}$. Since is can be very restrictive for area F, an upper-bound on an a priori knowledge of the current F_{cx} can also be used, instead of $F_{cx,\max}$. Note that the buoy and/or ballast can be instrumented to know their positions and so to simplify the model's evaluation. Angles between the boat and the umbilical and/or the ROV and the umbilical can also be measured using a camera for example.

Finally, a last practical problem is to recover the cable and the ROV after a deep sea mission. The cable l_1 (or l_0) spooling and the ROV's ascent must be synchronized to avoid any entanglement inside area C.

13. Conclusion

This work proposes three passive self-management strategies for the umbilical for an ROV, without motorized systems. Three configurations of the umbilical are proposed, each one to be the most adapted for different types of ROV exploration missions: near-surface, sea exploration, and diving in presence of large obstacles. Using moving ballasts and buoys to stretch the umbilical, a predictable shape of the cable in quasi-static equilibrium is provided while avoiding entanglements of the cable itself or with environmental obstacles. The model is exposed in 2 and 3 dimensions, considering the presence or absence of currents and waves. The choice of the ballasts and the buoys is described, to better counter-balance the effect of waves. The ROV's velocity is limited to keep the quasi-static equilibrium valid in all configurations. The forces applied on the umbilical and the ROV have been studied. Finally, experimentations have been performed in a pool, to show the validity of the method and the limits of the model.

If the hypothesis of quasi-static equilibrium is valid and not very binding for the ROV in a 2D plan, it can be very constraining in velocity for ROV's motions perpendicular to this plan. Thus, future works will study the dynamics instead of a quasi-static equilibrium, with also variations of the sea current and uncertainties on parameters. Finally, measurements at sea during a true mission will be performed.

Acknowledgment

We acknowledge support from the Centre National de la Recherche Scientifique (CNRS) and Laboratoire des sciences et techniques de l'information, de la communication et de la connaissance (Lab-STICC). The author declares that there is no conflict of interest.

References

[1] BA Abel. Underwater vehicle tether management systems. In *Proceedings of OCEANS'94*, volume 2, pages II–495, 1994.

[2] O. Blintsov. Development of the mathematical modeling method for dynamics of the flexible tether as an element of the underwater complex. *Eastern-European Journal of Enterprise Technologies*, 1 (7):4–14, 2017.

[3] L. Brignone, E. Raugel, J. Opderbecke, V. Rigaud, R. Piasco, and S. Ragot. First sea trials of hrov the new hybrid vehicle developed by ifremer. In *Oceans 2015-genova*, pages 1–7, 2015.

[4] B. Buckham and M. Nahon. Dynamics simulation of low tension tethers. In *IEEE Conference Proceedings Oceans*, volume 2, pages 757–766, 1999.

[5] R. D. Christ and R. L. Wernli Sr. *The ROV manual: a user guide for observation class remotely operated vehicles*. Elsevier, 2011.

[6] T. Crandle, G. Cook, and E. Celkis. Tradeoffs between umbilical and battery power in rov performance. In *IEEE OCEANS 2017-Anchorage*, pages 1–6, 2017.

[7] R. G. Duncan, Mark E. Froggatt, S. .T Kreger, R. J. Seeley, D. K. Gifford, A. K. Sang, and M. S. Wolfe. High-accuracy fiber-optic shape sensing. In *Sensor Systems and Networks*, volume 6530, page 65301S, 2007.

[8] O. A. Eidsvik and I. Schjølberg. Time domain modeling of rov umbilical using beam equations. *IFAC*, 49(23):452–457, 2016.

[9] O. A. N. Eidsvik and I. Schjølberg. Finite element cable-model for remotely operated vehicles (rovs) by application of beam theory. *Ocean Engineering*, 163:322–336, 2018.

[10] J. E. Frank, R. Geiger, D. R. Kraige, and A. Murali. Smart tether system for underwater navigation and cable shape measurement, 2013. US Patent 8,437,979, URL https://patents.google.com/patent/US8437979B2/en.

[11] O. Ganoni, R. Mukundan, and R. Green. Visually realistic graphical simulation of underwater cable. 2018.

[12] F. González, A. de la Prada, A. Luaces, and M. González. Real-time simulation of cable pay-out and reel-in with towed fishing gears. *Ocean Engineering*, 131:295–307, 2017.

[13] Sung Min Hong, Kyoung Nam Ha, and Joon-Young Kim. Dynamics modeling and motion simulation of usv/uuv with linked underwater cable. *Journal of Marine Science and Engineering*, 8(5):318, 2020.

[14] M. Laranjeira, C. Dune, and V. Hugel. Catenary-based visual servoing for tethered robots. In *IEEE International Conference on Robotics and Automation*, pages 732–738, 2017.

[15] M. Laranjeira, C. Dune, and V. Hugel. Embedded visual detection and shape identification of underwater umbilical for vehicle positioning. In *OCEANS 2019-Marseille*, pages 1–9, 2019.

[16] M. Laranjeira, C. Dune, and V. Hugel. Catenary-based visual servoing for tether shape control between underwater vehicles. *Ocean Engineering*, 200:107018, 2020.

[17] A. Lasbouygues, S. Louis, B. Ropars, L. Rossi, H. Jourde, H. Délas, P. Balordi, R. Bouchard, M. Dighouth, M. Dugrenot, et al. Robotic mapping of a karst aquifer. In *IFAC: International Federation of Automatic Control*, 2017.

[18] M. B. Lubis, M. Kimiaei, and M. Efthymiou. Alternative configurations to optimize tension in the umbilical of a work class rov performing ultra-deep-water operation. *Ocean Engineering*, 225:108786, 2021.

[19] H. Stuart, S. Wang, O. Khatib, and M. R. Cutkosky. The ocean one hands: An adaptive design for robust marine manipulation. *The International Journal of Robotics Research*, 36(2):150–166, 2017.

[20] M. Such, J. R. Jimenez-Octavio, A. Carnicero, and O. Lopez-Garcia. An approach based on the catenary equation to deal with static analysis of three dimensional cable structures. *Engineering structures*, 31(9):2162–2170, 2009.

[21] O. Tortorici, C. Anthierens, V. Hugel, and H. Barthelemy. Towards active self-management of umbilical linking rov and usv for safer submarine missions. *IFAC-PapersOnLine*, 52(21):265–270, 2019.

[22] Christophe Viel. Self-management of the umbilical of a rov for underwater exploration. https://hal.archives-ouvertes.fr/hal-03286654v2, 2021.

View publication stats